

# Retrieval of Colored Detrital Matter (CDM) light absorption coefficients in the Mediterranean Sea using field and satellite ocean color radiometry: Evaluation of bio-optical inversion models



Emanuele Organelli<sup>a,\*</sup>, Annick Bricaud<sup>a</sup>, Bernard Gentili<sup>a</sup>, David Antoine<sup>a,b</sup>, Vincenzo Vellucci<sup>a</sup>

<sup>a</sup> Sorbonne Universités, UPMC Univ Paris 06, CNRS, UMR 7093, Laboratoire d'Océanographie de Villefranche (LOV), 181 Chemin du Lazaret, 06230 Villefranche-sur-mer, France

<sup>b</sup> Curtin University, Department of Physics, Astronomy and Medical Radiation Sciences, Remote Sensing and Satellite Research Group, WA 6845 Perth, Australia

## ARTICLE INFO

### Article history:

Received 30 September 2014  
Received in revised form 5 August 2016  
Accepted 17 August 2016  
Available online xxxx

### Keywords:

Colored dissolved organic matter  
Colored Detrital Matter  
Ocean color inversion  
Bio-optical models  
Carbon dynamics  
Mediterranean Sea

## ABSTRACT

Quantifying Colored Detrital Matter (CDM) from satellite observations can improve our knowledge of carbon dynamics in coastal areas and the open oceans. Several bio-optical inversion models have been developed for this purpose. However, care must be taken when they are applied to waters where optical properties significantly differ from model assumptions, which is the case in the Mediterranean Sea. Algorithm testing and validation are thus required before routine use. Here, *in situ* radiometric measurements collected in the NW Mediterranean Sea (BOUSSOLE site) are used to evaluate three bio-optical inversion models that retrieve the CDM light absorption coefficients at 443 nm ( $a_{\text{cdm}}(443)$ ). Although all methods reproduced the CDM seasonal cycles at the surface, comparisons of predicted and *in situ*  $a_{\text{cdm}}(443)$  coefficients showed that the Quasi-Analytical Algorithm version 6 (QAAv6) and a locally-adapted version of the Garver-Siegel-Maritorena model (GSM-Med) were the two best algorithms. Applying these two models to SeaWiFS remote sensing reflectances, collected between 2003 and 2010, reproduced with good accuracy the  $a_{\text{cdm}}(443)$  coefficients retrieved from field radiometric measurements at the BOUSSOLE site, with seasonal patterns consistent with previous observations. Finally, bio-optical relationships derived from satellite-retrieved  $a_{\text{cdm}}(443)$  and chlorophyll values confirmed the higher-than-average CDM contribution for a given chlorophyll concentration in the Mediterranean Sea as compared to many oceanic regions.

© 2016 Elsevier Inc. All rights reserved.

## 1. Introduction

The spatio-temporal dynamics of the organic material dissolved or suspended as particulates in the oceans reflects the functioning of the carbon cycle. Colored dissolved organic matter (CDOM) is a fraction of the total dissolved organic material (DOM), and its specific optical properties (*i.e.*, decreasing exponential shape of light absorption; Bricaud *et al.*, 1981) allow it to be observed at global scale by remote-sensing platforms. CDOM light absorption properties are distinguishable from those of phytoplankton, and they show spectral features similar to non-algal particles (NAP). Colored Detrital Matter (CDM) is defined as the sum of CDOM and NAP.

Bio-optical inversion algorithms can retrieve CDOM and, more often, CDM light absorption coefficients from apparent optical properties such as sea surface reflectance. Some of these algorithms were developed for coastal waters or areas strongly influenced by river discharge, which contain a considerable amount of CDOM and CDM of terrestrial origin (D'Sa and Miller, 2003; Bélanger *et al.*, 2008; Mannino *et al.*, 2008;

Maselli *et al.*, 2009; Zhu *et al.*, 2011; Matsuoka *et al.*, 2013; Mannino *et al.*, 2014). Other algorithms retrieve CDOM and CDM absorption coefficients in oceanic waters, where their content is generally low and of local and biologically driven origin (Coble, 2007). These algorithms are based on reflectance ratios (Morel and Gentili, 2009a; Shanmugam, 2011) and anomalies (Brown *et al.*, 2008), multivariate statistical techniques (Cao and Miller, 2015) or consist of semi-analytical approaches that estimate the CDM absorption coefficients at several wavelengths together with other bio-optical quantities (Hoge and Lyon, 1996; Carder *et al.*, 1999; Lee *et al.*, 2002; Maritorena *et al.*, 2002; Boss and Roesler, 2006; Ciotti and Bricaud, 2006; Devred *et al.*, 2006).

These semi-analytical approaches and their uncertainties were compared using the International Ocean-Colour Coordinating Group dataset (IOCCG, 2006). The Lee *et al.* (2002) and Maritorena *et al.* (2002) methods were the two best algorithms for retrieving the absorption coefficients of CDM. They are used for estimating the CDM absorption coefficients at the global (*e.g.*, Siegel *et al.*, 2002, 2005, 2013; Lee *et al.*, 2009; Maritorena *et al.*, 2010) and regional (*e.g.*, Kostadinov *et al.*, 2007; Nagamani *et al.*, 2011; Dong *et al.*, 2013; Huang *et al.*, 2013; Kahru *et al.*, 2013; Matsuoka *et al.*, 2013; Zheng *et al.*, 2014) scales. The Ciotti and Bricaud (2006) method also showed reasonable accuracy in retrieving the CDM absorption coefficient at 443 nm and in

\* Corresponding author at: Plymouth Marine Laboratory, Prospect Place, The Hoe, PL1 3DH Plymouth, United Kingdom.

E-mail address: [emo@pml.ac.uk](mailto:emo@pml.ac.uk) (E. Organelli).

reproducing its seasonal dynamics at the global and basin scales from satellite data (Bricaud et al., 2012). However, all the semi-analytical bio-optical models fail or perform poorly when they are applied to regions with distinctive optical properties for which the algorithms are not designed (IOCCG, 2006; Kostadinov et al., 2007; Shanmugam et al., 2010; Huang et al., 2013). It follows that these models should be tested and locally tuned before being applied to specific areas.

Algorithm testing and validation is essential to improve the retrieval of CDOM and CDM light absorption coefficients in the Mediterranean Sea. The peculiar bio-optical properties of this basin make its low-chlorophyll waters appear greener than expected (Claustre et al., 2002; Morel and Gentili, 2009b). Possible causes of this optical behavior include Saharan dust suspended in the surface layer (Claustre et al., 2002), a higher abundance of coccolithophores with respect to other algal groups (Gitelson et al., 1996; D'Ortenzio et al., 2002) or a high CDOM content (Morel and Gentili, 2009b; Organelli et al., 2014). In particular, CDOM absorption dominates over phytoplankton and non-algal particle absorption during almost all seasons in the blue region of the spectrum (Organelli et al., 2014). This high CDOM contribution might lead bio-optical inversion models to fail if they were validated at the global scale.

This study evaluates three semi-analytical inversion models (Lee et al., 2002; Maritorena et al., 2002; Ciotti and Bricaud, 2006) for the retrieval of CDM light absorption coefficients at 443 nm ( $a_{\text{cdm}}(443)$ ) in Mediterranean waters using *in situ* remote sensing reflectances measured over three years at the *BOUée pour l'acquiSition d'une Série Optique à Long termE* (BOUSSOLE) site (NW Mediterranean Sea; Antoine et al., 2006). Specific model assumptions are compared to *in situ* inherent optical properties (IOPs) to understand how the bio-optical inversion algorithms perform when applied to the BOUSSOLE dataset. Locally-tuned configurations of the algorithms are also presented and discussed. The best algorithms are then used to reproduce  $a_{\text{cdm}}(443)$  temporal variations at the BOUSSOLE site using eight years of *in situ* and *Sea-viewing Wide Field-of-view Sensor* (SeaWiFS; Hooker et al., 1992) radiometric measurements. Finally, validated satellite-derived time-series are used to investigate seasonal dynamics of  $a_{\text{cdm}}(443)$

coefficients for the BOUSSOLE time-series and to assess bio-optical relationships with algal chlorophyll concentrations.

## 2. Material and methods

### 2.1. Study area

The BOUSSOLE site is located in the Ligurian Sea at 7°54'E, 43°22'N (NW Mediterranean Sea; Fig. 1), about 32 nautical miles off the French Riviera coast. The water depth is 2440 m at the mooring point. BOUSSOLE is a long-term time-series of optical quantities and has been active since July 2001. BOUSSOLE is a Case-1 water site according to the definition of Morel and Prieur (1977), as stated by Antoine et al. (2008) and Organelli et al. (2014). Details on the sampling strategy can be found in Antoine et al. (2006) and at the URL <http://www.obs-vlfr.fr/Boussole/>. Briefly, a buoy specifically designed for collecting radiometric and bio-optical quantities was deployed at the mooring site and collects data at high frequency (every 15 min) night and day at two fixed depths (4 and 9 m). Recorded quantities include downward and upward irradiances and upwelling radiance at nadir, chlorophyll fluorescence, as well as backscattering and beam attenuation coefficients. A monthly cruise provides a complementary dataset of vertical profiles of irradiance, algal pigment concentrations and IOPs (CDOM and particulate light absorption coefficients).

### 2.2. In situ data acquisition for testing bio-optical models

#### 2.2.1. Sampling

Seawater was sampled at various depths within the 0–400 m water column by a rosette system equipped with 12-L Niskin bottles during up-cast CTD measurements. Water sub-samples were used for the determination of algal pigment concentrations, CDOM and particulate light absorption coefficients. In this study, only samples collected within the first optical depth (generally at 5 and 10 m) were averaged and used for match-up and time-series analyses. Following Morel (1988), the first optical depth was computed as  $Z_{\text{eu}}/4.6$  where the euphotic depth,  $Z_{\text{eu}}$ , is

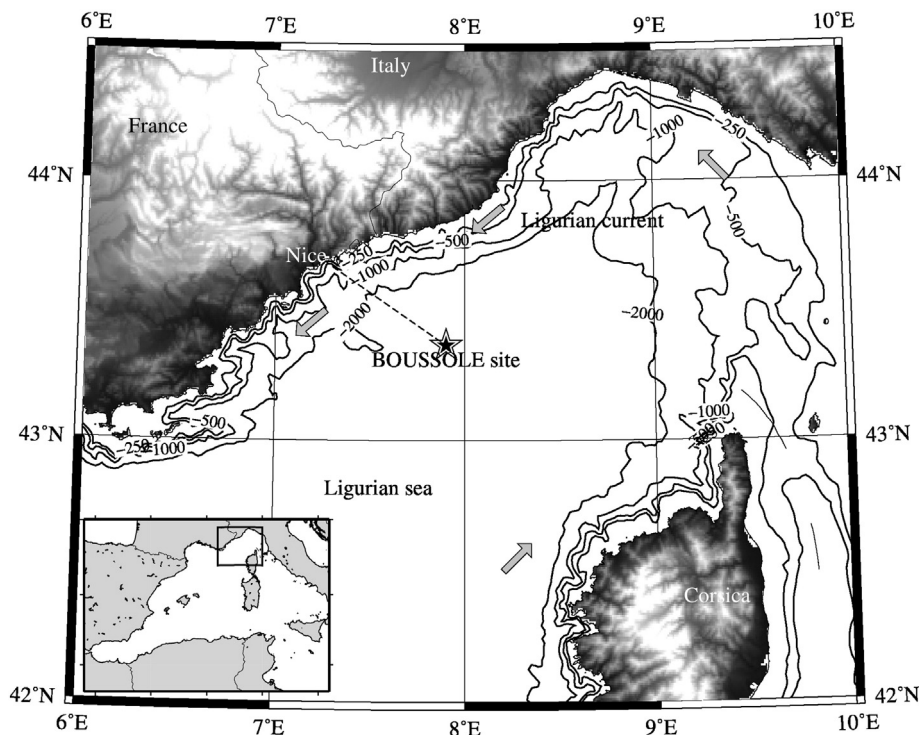


Fig. 1. Area in the Mediterranean Sea where the BOUSSOLE site is located (black star). Gray arrows show the main current flow.

the depth at which photosynthetically available radiation (PAR) is reduced to 1% of its value just below the sea surface. The euphotic depth was estimated from measured chlorophyll profiles according to Morel and Maritorena (2001).

### 2.2.2. Pigment measurements

Seawater sub-samples (2.8 L) were filtered through 0.7  $\mu\text{m}$  GF/F Whatman filters (25 mm  $\phi$ ) and immediately frozen in liquid nitrogen and then stored in a  $-80^\circ\text{C}$  laboratory freezer until analysis. Chlorophyll *a* concentrations were determined together with other algal pigments by high performance liquid chromatography (HPLC) according to the analytic procedure described in Ras et al. (2008). The sum of chlorophyll *a*, divinyl-chlorophyll *a* and chlorophyllide *a* is used as an index of phytoplankton biomass and is referred to as [Tchl *a*]. Pigment measurements were performed monthly from September 2003 to December 2013.

### 2.2.3. Light absorption measurements

The methodology used for CDOM absorption measurements is described in Organelli et al. (2014). Briefly, seawater sub-samples were immediately filtered after sampling into glass bottles through pre-rinsed 0.2  $\mu\text{m}$  GHP filters (Acrodisc Inc.) and were kept refrigerated until the analysis. Samples were allowed to warm up at room temperature at the time of the analysis. All samples were analyzed within 24 h after sampling according to the Ocean Optics Protocols (Mitchell et al., 2002). CDOM absorption measurements were performed using a multiple path length, liquid core waveguide, UltraPath system (World Precision Instruments, Inc.). All absorbance spectra were measured between 250 and 735 nm (1-nm increments) with reference to a salt solution (38 g  $\text{L}^{-1}$ ) using a 200-cm path length. Measured spectra were corrected for residual absorbance in the near infrared, if any, by assuming that the average of measured values over a 5 nm interval around 685 nm must be 0 and shifting the spectra accordingly (samples were disregarded if this value was  $>0.02$  AU). Finally, the corrected absorbance spectra were transformed into absorption coefficients,  $a_{\text{cdom}}$  (in  $\text{m}^{-1}$ ). CDOM absorption measurements were available monthly for three years of the BOUSSOLE time-series (i.e., Jan. 2011 to Dec. 2013).

Particulate light absorption spectra,  $a_p(\lambda)$ , were measured using the “quantitative filter pad technique (QFT)” (Mitchell, 1990; Mitchell et al., 2000). Seawater sub-samples (2.8 L) were filtered using a 0.7  $\mu\text{m}$  Whatman GF/F filter (25 mm  $\phi$ ) and immediately stored in liquid nitrogen, and then stored in a  $-80^\circ\text{C}$  laboratory freezer until analysis. Particulate absorption measurements were performed using a Perkin-Elmer Lambda 19 spectrophotometer, and a Lambda 850 (from January 2011), and both were equipped with an integrating sphere. The consistency of measurements provided by the two spectrophotometers was checked on duplicate measurements throughout the year of 2011 (J. Ras and M. Ouhssain, unpublished results). Absorbance spectra were measured between 300 and 800 nm (1-nm increments) for filters positioned at the entrance of the integrating sphere, with a blank wet filter as a reference. Measured optical densities were shifted to 0 in the red part of the spectrum, and then they were converted into absorption coefficients (in  $\text{m}^{-1}$ ). All spectra were corrected for the path length amplification factor according to Bricaud and Stramski (1990). Finally, the particulate absorption spectra were decomposed into phytoplankton ( $a_{\text{phy}}(\lambda)$ ) and non-algal particle ( $a_{\text{NAP}}(\lambda)$ ) absorption coefficients using the numerical decomposition technique described in Bricaud and Stramski (1990). Phytoplankton light absorption coefficients were converted into chlorophyll-specific light absorption coefficients ( $a_{\text{phy}}^*(\lambda)$ ) by normalizing to [Tchl *a*]. Particulate absorption measurements were performed monthly from September 2003 to December 2013.

Light absorption coefficients of Colored Detrital Matter ( $a_{\text{cdm}}(\lambda)$ ) were calculated as the sum of the CDOM and non-algal particle absorption coefficients over the 300–735 nm range (1-nm increments) for the period January 2011–December 2013. The spectral slope ( $S_{\text{cdm}}$ , in

$\text{nm}^{-1}$ ) was computed by applying a non-linear least-square fit to the  $a_{\text{cdm}}(\lambda)$  values between 350 and 500 nm (Babin et al., 2003):

$$a_{\text{cdm}}(\lambda) = a_{\text{cdm}}(\lambda_0) \exp^{-S_{\text{cdm}}(\lambda-\lambda_0)} \quad (1)$$

where  $a_{\text{cdm}}(\lambda_0)$  is the CDM absorption value at a reference wavelength (440 nm).

### 2.2.4. Backscattering measurements

The angular scattering coefficient at  $140^\circ$ ,  $\beta(140)$ , was measured every 15 min by a Hydrosat-4 backscattering meter (HOBI Labs) installed on the permanent buoy at 9 m depth. The instrument collected data at 442, 488, 550 and 620 nm. Detailed procedures for the calculation of the particle backscattering coefficient ( $b_{\text{bp}}(\lambda)$ ) are described in Antoine et al. (2011).

The spectral slope ( $\gamma$ ), describing the spectral dependency of  $b_{\text{bp}}(\lambda)$ , was calculated as

$$\gamma = -\log(b_{\text{bp}}(\lambda_1)/b_{\text{bp}}(\lambda_2)) / \log(\lambda_1/\lambda_2) \quad (2)$$

with  $\lambda_1 = 442$  nm and  $\lambda_2 = 620$  nm. Only backscattering measurements collected between 2008 and 2011 at the BOUSSOLE site were available at these wavelengths.

## 2.3. Radiometry measurements

### 2.3.1. Field measurements and data processing

**2.3.1.1. Vertical profiles.** A Compact Optical Profiling System (C-OPS; Biospherical Instrument Inc.) was deployed monthly since January 2011 for measuring upward irradiance profiles (within 0–150 m). An above-water reference sensor of incident solar irradiance ( $E_s$ ) was operated simultaneously with the underwater profiler. The two radiometers were factory calibrated yearly. Measurements were taken for 18 channels, but only the wavelengths closest to the SeaWiFS bands were used in this study (i.e., 412, 443, 490, 510, 555 and 665 nm), and only kept when the instrument tilt was lower than  $5^\circ$ . The C-OPS was deployed within 1 h of water sampling, around solar noon, under clear or overcast sky conditions and wind generally below 15 kn. Each profile was repeated from 3 to 6 times and used to calculate the Remote Sensing Reflectance ( $R_{\text{rs}}(\lambda)$ ). The  $R_{\text{rs}}(\lambda)$ -derived  $a_{\text{cdm}}(\lambda)$  values were then averaged and the standard deviation was computed. Finally, 87 profiles corresponding to 25 water-sampling days providing  $a_{\text{cdm}}(\lambda)$  values at the sea surface were available for the period from January 2011 to December 2013.

The Remote Sensing Reflectance,  $R_{\text{rs}}(\lambda)$  (in  $\text{sr}^{-1}$ ), defined as the ratio between the water-leaving radiance ( $L_w$ ) and  $E_s$  was calculated as (the wavelength dependence is omitted for brevity)

$$R_{\text{rs}} = L_w/E_s \quad (3)$$

where  $L_w$  is calculated from the upward irradiance just below the sea surface ( $E_u(0^-)$ ):

$$L_w = E_u(0^-) * \left( (1-\rho)/n^2 \right) * 1/Q(\theta, \text{Tchl } a) \quad (4)$$

In Eq. (4),  $\rho$  is the Fresnel reflection coefficient for the water-air interface,  $n$  is the refractive index of seawater and  $Q(\theta, \text{Tchl } a)$  is the ratio of upward irradiance to upward radiance below the surface (i.e.,  $E_u(0^-)/L_u(0^-)$ ). The  $Q(\theta, \text{Tchl } a)$  value was log-linearly interpolated from look-up tables, as provided in Morel et al. (2002), to match the solar zenith angle ( $\theta$ ) of each measurement and the Tchl *a* content from the closest available surface discrete chlorophyll concentration (note that a linear interpolation of the  $Q(\theta, \text{Tchl } a)$  factor was also used to match the instrument wavelength). Upward irradiance values were extrapolated to null depth ( $E_u(0^-)$ ) by a quadratic fit to the  $E_u(z)$

profile. The fit included  $E_u(z)$  values from the  $0^-$  level down to the depth where  $E_u(z)$  was reduced to 25% of its surface ( $0^-$ ) value. This procedure was established from analyzing a large dataset of radiometric profiles collected with a SeaWiFS Profiling Multichannel Radiometer (SPMR; Satlantic Inc.) at the BOUSSOLE site from 2001 to 2010. The  $E_u(0^-)$  obtained in this way was compared to its value directly measured by hanging the  $E_u$  radiometer head just below the surface. The  $E_u(0^-)$  estimates from the second-degree polynomial fit were closer to the true values than those obtained by the usual log-linear extrapolations (Mueller et al., 2003; D. Antoine and B. Gentili, unpublished results). Before calculating  $R_{rs}(\lambda)$  (Eq. (3)),  $E_u(0^-)$  values were corrected for instrument self-shading according to Gordon and Ding (1992).

**2.3.1.2. Buoy measurements.** A set of Satlantic 200-Series radiometers collected simultaneous measurements of above-water surface irradiance ( $E_s(\lambda)$ ) and in-water upward radiance ( $L_u(\lambda)$ ) at 4 and 9 m depth. All measurements were acquired at 6 wavelengths (i.e., 412, 443, 490, 510, 560 and 670 nm) every 15 min. A Seabird SBE37 CTD mounted in the core of the buoy structure provided the reference depth for the radiometers.

The procedures used for data processing are described in detail by Antoine et al. (2006, 2008). Briefly, to calculate  $R_{rs}(\lambda)$  (Eq. (3)),  $L_w$

was derived from upward nadir radiance measurements:

$$L_w = L_u(0^-) \left( (1-\rho)/n^2 \right) \quad (5)$$

where  $\rho$  is the Fresnel reflection coefficient for the water-air interface and  $n$  is the refractive index of seawater.  $L_u(0^-)$  is the upward radiance just below the sea surface and was calculated as

$$L_u(0^-) = L_u(z) e^{zK_L} \quad (6)$$

where  $z$  is the shallowest measurement depth for  $L_u$ . The diffuse attenuation coefficient,  $K_L$ , was computed from measurements at 4 and 9 m as follows:

$$K_L = -\ln(L_u(z_2)/L_u(z_1))/(z_2-z_1) \text{ with } z_2 > z_1 \quad (7)$$

Before calculating  $R_{rs}(\lambda)$  (Eq. (3)),  $L_u(0^-)$  values were corrected for instrument self-shading (Gordon and Ding, 1992). In addition, because  $L_u(0^-)$  values could be improperly determined when extrapolated to  $0^-$  from an average depth of 4 m (Antoine et al., 2008), the extrapolated values were corrected through look-up tables derived from radiative transfer simulations (see Appendix A in Antoine et al., 2008).

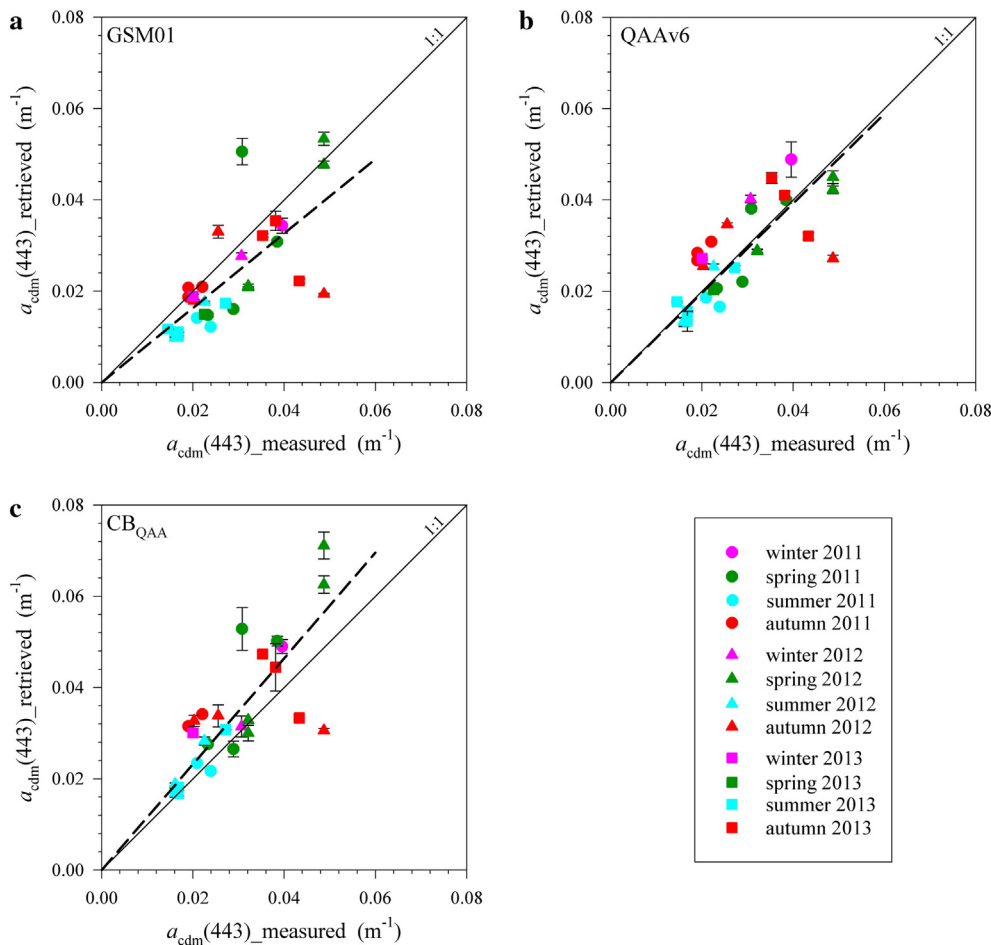


**Fig. 2.** Comparison between  $a_{\text{cdm}}(443)$  coefficients as derived from radiometric measurements (C-OPS and buoy) and as measured from water sampling at the BOUSSOLE site (January 2011–December 2013), for the following inversion algorithms: a) GSM01; b) QAAv6; and c)  $\text{CB}_{\text{QAA}}$ . Each  $a_{\text{cdm}}(443)$  estimate is the average value for at least three independent  $R_{rs}(\lambda)$  measurements and error bars are the standard deviation values. In each plot, the solid line is the 1:1 line and the dashed line is a linear fit to all points. Regression statistics are displayed in Table 1.

**Table 1**  
Statistics for match-up analyses shown in Fig. 2 (see Section 2.4 for definitions).

Method	n	Valid retrievals <sup>a</sup>			b (y = bx)	r <sup>2</sup>	p-Value	S <sub>err</sub>	RMSE	MPD	RMSE <sub>log</sub>
		C-OPS	Buoy	Total							
GSM01	30	99%	97%	97%	0.816	0.90	<0.001	0.051	0.010	30.88%	0.176
QAAv6	30	100%	99%	99%	0.981	0.94	<0.001	0.045	0.007	21.12%	0.109
CB <sub>QAA</sub>	27	72%	43%	44%	1.159	0.94	<0.001	0.056	0.010	23.09%	0.126

<sup>a</sup> The number of valid retrievals was computed considering all C-OPS ( $n = 87$ ) and buoy ( $n = 2606$ ) measurements collected over the time-series between January 2011 and December 2013.

Data processing also included verification and correction of data corrupted by biofouling (*i.e.*, growth of organisms on the radiometers) according to Antoine et al. (2008). Moreover, the set of Satlantic 200-Series radiometers was replaced about every six months with an identical set of instruments but with a few changes in wavelengths (*i.e.*, 443, 490, 511, 555, 560, 665 and 683 nm). Additional selection criteria were as follows: the buoy tilt was  $<10^\circ$ , the buoy CTD depth was  $<11$  m to ensure the  $E_s$  radiometer was above water, and the ratio of the measured  $E_s(490)$  to the theoretical clear-sky value (Gregg and Carder, 1990) varied between 0.8 and 1.25. Finally, only data collected around solar noon (10 am–2 pm, GMT) were selected and used to calculate  $R_{rs}(\lambda)$ .  $R_{rs}(\lambda)$ -derived  $a_{cdm}(\lambda)$  values were then averaged and the standard deviation was computed. A total of 6676  $R_{rs}(\lambda)$  spectra, measured between September 2003 and July 2013, were used in the present study.

The quality of radiometric measurements from the buoy and the uncertainties are described in Antoine et al. (2006, 2008). They found highly significant relationships with a bias of approximately 2% (Antoine et al., 2006) between normalized  $L_w$  values derived from the buoy and from a Satlantic SPMR radiometric profiler. The consistency of the reflectance measurements provided by the SPMR and the C-OPS profiler used in this study was verified by performing simultaneous casts throughout the year 2010 ( $y = 1.017x$ ,  $r^2 = 0.99$ , RMSE = 0.00261,  $n = 368$ ,  $p < 0.001$ , all wavelengths combined).

### 2.3.2. Satellite data

Level 3 SeaWiFS 8-day products with a spatial resolution of 9.2 km at the Equator (processing version R2010.0) were downloaded from the

NASA ocean color website (<http://oceancolor.gsfc.nasa.gov/>) for the period from January 2003 to December 2010.

Remote sensing reflectances at six wavelengths (412, 443, 490, 510, 555 and 670 nm) extracted for non-flagged pixels across the Mediterranean basin ( $5^\circ\text{W}$ – $37^\circ\text{E}$ ,  $30^\circ\text{N}$ – $46^\circ\text{N}$ ) were used to estimate  $a_{cdm}(443)$  coefficients. SeaWiFS-derived light absorption coefficients and chlorophyll concentrations (provided by the OC4v6 algorithm) for a  $3 \times 3$  pixel array centered on the BOUSSOLE site were averaged for comparison with  $a_{cdm}(443)$  time-series derived from radiometric buoy measurements between 2003 and 2010. The consistency between buoy and SeaWiFS reflectances was discussed in Antoine et al. (2008).

### 2.4. Bio-optical inversion models

The Garver-Siegel-Maritorena method (GSM) is a semi-analytical bio-optical model originally developed by Garver and Siegel (1997) and then optimized by Maritorena et al. (2002) for ocean color applications at the global scale. This algorithm, which is based on the relationship between  $R_{rs}(\lambda)$  and IOPs according to Gordon et al. (1988), uses a non-linear least-squares technique to fit  $R_{rs}(\lambda)$  and to derive the chlorophyll concentration and the magnitudes of CDM light absorption and particle backscattering coefficients at 443 nm. In addition to absorption and backscattering coefficients of pure seawater, spectral shapes are fixed for the chlorophyll-specific phytoplankton light absorption ( $a^*_{phy}(\lambda)$ ), the CDM light absorption and the particle light backscattering coefficients (Maritorena et al., 2002). The version of the algorithm updated by Maritorena et al. (2002) and extended to six bands (*i.e.*,

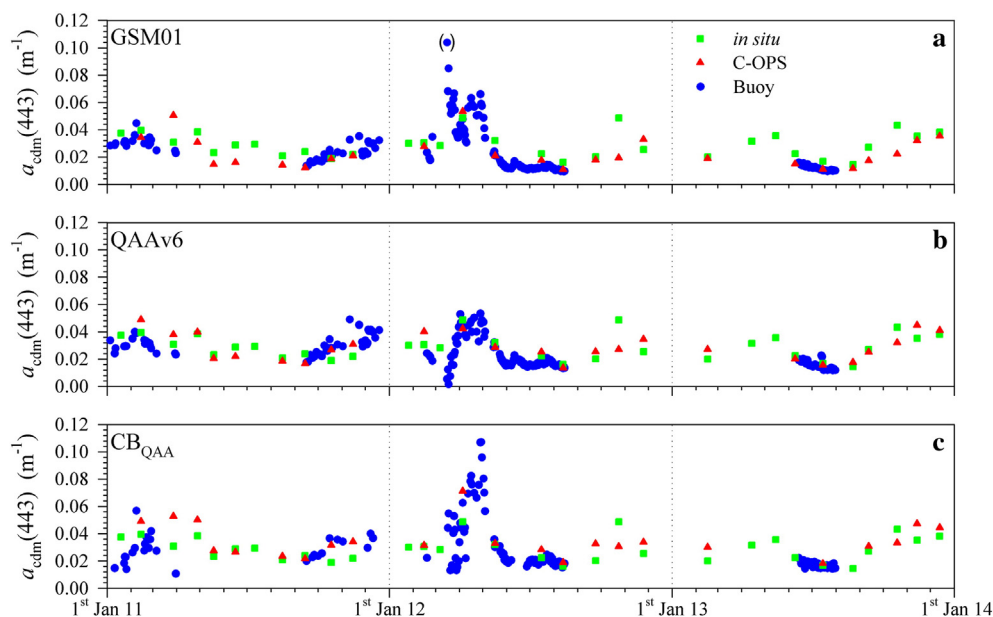


**Fig. 3.** BOUSSOLE time-series (January 2011–December 2013) of  $a_{cdm}(443)$  coefficients as measured at sea and as retrieved from C-OPS and buoy radiometric measurements using the following inversion algorithms: a) GSM01; b) QAAv6; and c) CB<sub>QAA</sub>. In panel (a), parentheses indicate  $a_{cdm}(443)$  estimates outside of the y-axis range.

412, 443, 490, 510, 555, and 670 nm) is tested here, and called GSM01 as in Maritorena et al. (2002).

The Quasi-Analytical Algorithm (QAA) was originally developed by Lee et al. (2002) and then updated by Lee et al. (2007; version 4) and Lee et al. (2009; version 5). It uses an analytical inversion of  $R_{rs}(\lambda)$  to retrieve IOPs, i.e., the total light absorption and backscattering coefficients. These coefficients are estimated at a reference wavelength ( $\lambda = 555$  nm) and then the calculation is propagated to other wavelengths by modeling the spectral shape of the backscattering coefficient (Lee et al., 2009). Finally, the backscattering spectrum is used through Eq. (5) of Lee et al. (2002) to derive the total absorption coefficient (see details in Lee et al., 2002; IOCCG, 2006). This absorption spectrum is then decomposed into CDM and phytoplankton contributions, following a spectral model based on the variability of the 412/443 nm band ratios

both for CDM and phytoplankton absorption coefficients (and for the CDM exponential slope since version 5; Lee et al., 2009). Version 6 of the algorithm for SeaWiFS bands, which is currently integrated in the SeaWiFS data analysis system (SeaDAS, released by NASA), is tested here and called QAAv6. This update extends the calculation to more turbid waters, while it is the same as version 5 for oceanic areas (Z.P. Lee, Personal communication; [http://www.ioccg.org/groups/Software\\_OCA/QAA\\_v6\\_2014209.pdf](http://www.ioccg.org/groups/Software_OCA/QAA_v6_2014209.pdf)).

The Ciotti and Bricaud method (CB2006) was originally developed by Ciotti and Bricaud (2006) and revised by Bricaud et al. (2012; CB2012). CB2012 starts with deriving the total absorption coefficients at four wavelengths (i.e., 412, 443, 490 and 510 nm) from  $R_{rs}(\lambda)$  by using the Loisel and Stramski algorithm (Loisel and Stramski, 2000; Loisel and Poteau, 2006). Then, a non-linear optimization technique is

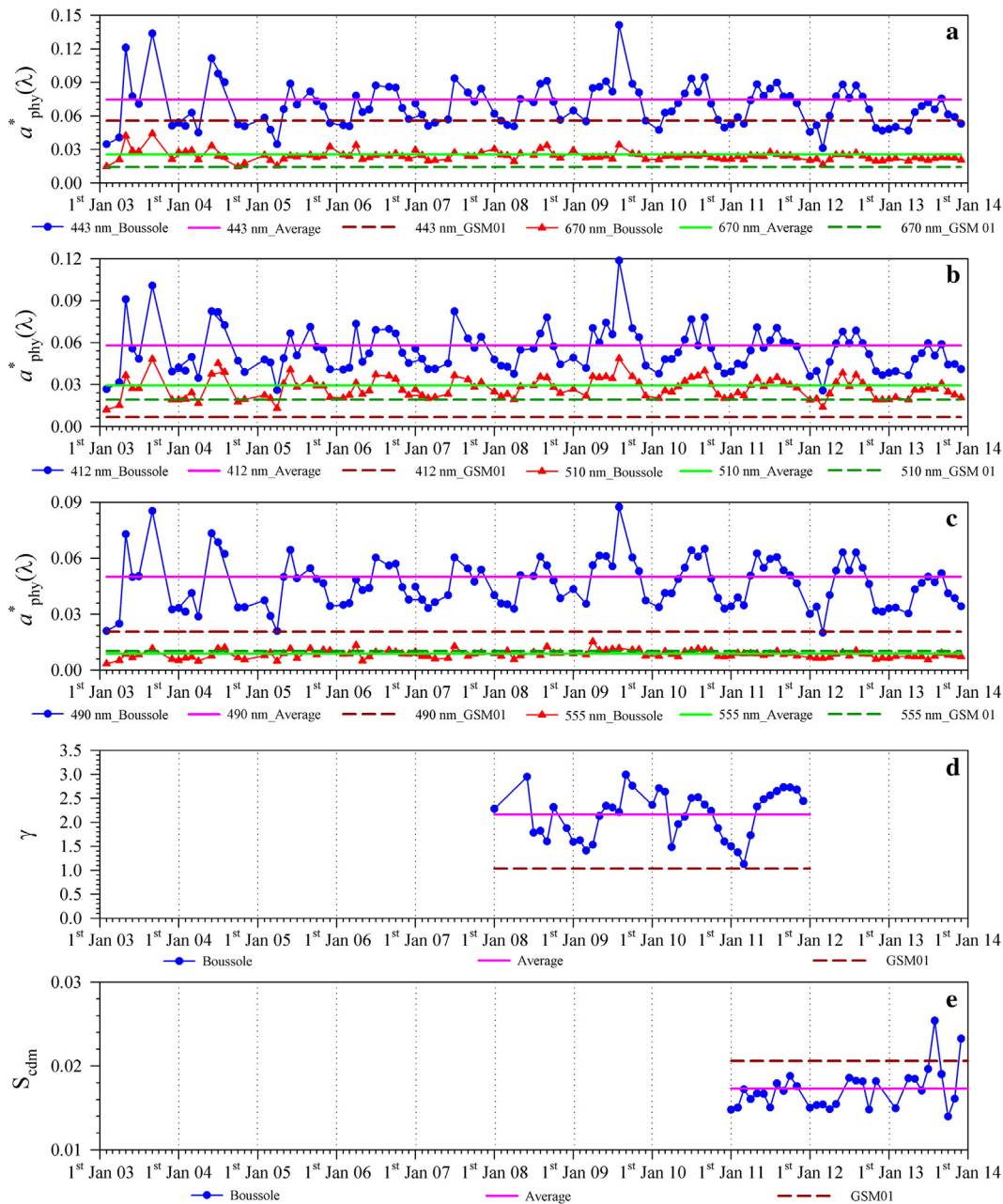


**Fig. 4.** Monthly time-series within the first optical depth at the BOUSSOLE site: a–c) chlorophyll-specific phytoplankton light absorption coefficients ( $a_{phy}^*(\lambda)$ ) at 412, 443, 490, 510, 555 and 670 nm collected between January 2003 and December 2013; d) spectral dependency of particle light backscattering coefficient ( $\gamma$ ) measured between January 2008 and December 2011; and e) spectral dependency of Colored Detrital Matter light absorption coefficients ( $S_{cdm}$ ) measured between January 2011 and December 2013. In each plot, the average of each variable over the time-series at the BOUSSOLE site and the values used by the GSM01 algorithm (updated by Maritorena et al., 2002) are shown for comparison.

used to derive the  $a_{\text{cdm}}(443)$  coefficient, the spectral slope of CDM light absorption and a size factor for phytoplankton (Ciotti et al., 2002), by forcing the output values to vary in the ranges  $[0-10 \text{ m}^{-1}]$ ,  $[0-0.05 \text{ nm}^{-1}]$  and  $[-0.5 \text{ to } 1.5]$ , respectively. Convergence between observed and simulated  $R_{\text{rs}}(\lambda)$  was assumed when the difference (see equation 11 in Ciotti and Bricaud, 2006) was  $<0.05$ . As the Loisel and Stramski method fails to retrieve total absorption coefficients in the clearest waters (Bricaud et al., 2012), it is replaced here by the QAAv6 and the values at 510 nm are dropped out of the non-linear optimization (performed at three wavelengths only, i.e., 412, 443 and 490 nm). This version of the algorithm is hereafter called CB<sub>QAA</sub>.

The performance of these bio-optical models was evaluated through match-up analyses with *in situ* data by calculating the root mean square error of prediction (RMSE):

$$RMSE = \sqrt{\frac{\sum_{i=1}^n (x_{i,\text{estimated}} - x_{i,\text{measured}})^2}{n}} \quad (8)$$

and the median percent difference (MPD) calculated as (Werdell et al., 2013)

$$MPD = \text{median} \left( 100 * \frac{x_{i,\text{estimated}}}{x_{i,\text{measured}}} - 1 \right) \quad (9)$$

where  $x$  is the variable and  $n$  is the number of observations. To compare the results of GSM01 and QAAv6 with the International Ocean-Colour Coordinating Group (IOCCG, 2006), RMSE was also computed for the log-transformed quantities:

$$RMSE_{\log} = \sqrt{\frac{\sum_{i=1}^n (\log(x_{i,\text{estimated}}) - \log(x_{i,\text{measured}}))^2}{n-2}} \quad (10)$$

The coefficient of determination ( $r^2$ ), slope ( $b$ ) and standard error ( $S_{\text{err}}$ ) of linear regressions were also computed. The relative number of valid retrievals (i.e., when the  $R_{\text{rs}}$  spectrum yielded a valid result according to the model constraints) was also determined. In this study, we only evaluated the ability of each algorithm to predict  $a_{\text{cdm}}(443)$  coefficients.

### 3. Results and discussion

The three bio-optical models retrieved  $a_{\text{cdm}}(443)$  coefficients at the BOUSSOLE site with different accuracies: MPD values varied between 21.12% for QAAv6 to 30.88% for GSM01 (Fig. 2; Table 1). The percentage of valid retrievals was also different, from 44% for CB<sub>QAA</sub> to 99% for QAAv6 (Table 1). However, all the algorithms reproduced the temporal variability of *in situ*  $a_{\text{cdm}}(443)$  coefficients for the BOUSSOLE time-series between 2011 and 2013, using both C-OPS and buoy radiometric measurements (Fig. 3). Details on each bio-optical model are presented separately in the following sections. The discussion is focused on understanding the reasons why the tested bio-optical inversion algorithms performed differently. Then, the best *in situ* algorithms were applied to eight years of SeaWiFS radiometric measurements, and the results are discussed to investigate  $a_{\text{cdm}}(443)$  temporal dynamics and relationships with chlorophyll concentrations at the local scale.

#### 3.1. GSM01

The GSM01 (Maritorena et al., 2002) underestimated the  $a_{\text{cdm}}(443)$  values for the BOUSSOLE time-series with RMSE and MPD of  $0.010 \text{ m}^{-1}$  and 30.88%, respectively (Fig. 2a; Table 1). This result contrasted with the IOCCG (2006) and Siegel et al. (2013) for applications at the global scale, but agreed with Huang et al. (2013) for more coastal areas. Although the error for log-transformed quantities observed for the

BOUSSOLE site ( $RMSE_{\log} = 0.176$ ) was lower than the error observed for the *in situ* IOCCG (2006) dataset ( $RMSE_{\log} = 0.246$ ), this version of the algorithm was not suitable for estimating  $a_{\text{cdm}}(443)$  coefficients at the BOUSSOLE site.

The low accuracy resulted from the discrepancy between model assumptions and field surface observations at the BOUSSOLE site. There were large differences between the average *in situ* values of  $a^*_{\text{phy}}(\lambda)$ ,  $\gamma$  and  $S_{\text{cdm}}$  and the values used in GSM01 (Fig. 4). The BOUSSOLE site had higher  $a^*_{\text{phy}}(\lambda)$  values than GSM01 (Fig. 4a–c), except for the 555 nm band (Fig. 4c). These differences were expected given the inverse relationship between  $a^*_{\text{phy}}(\lambda)$  values and cell size (Bricaud et al., 1995, 1998; Organelli et al., 2011). The phytoplankton community at the BOUSSOLE site was dominated by small cells (Organelli et al., 2013) with high  $a^*_{\text{phy}}(\lambda)$  values from late spring to autumn (Fig. 4a–c). By contrast, the  $a^*_{\text{phy}}(\lambda)$  used in GSM01 are representative of large phytoplankton cells with low  $a^*_{\text{phy}}(\lambda)$  values (Maritorena et al., 2002 and references therein).

Similarly, the high average  $\gamma$  value (Fig. 4d) at the BOUSSOLE site indicated a larger amount of small particles (see also Antoine et al., 2011) compared with the GSM01 configuration (Maritorena et al., 2002). The lower average  $S_{\text{cdm}}$  value at the BOUSSOLE site (Fig. 4e) suggested a different CDM origin/nature and the influence of photochemical/microbial degradation processes compared with the GSM01 configuration. Hence, GSM01 performed poorly because the modeled IOPs (Maritorena et al., 2002) were representative of an ecosystem different from the BOUSSOLE site.

A version of the GSM01 algorithm was then adapted with locally-tuned values (hereafter called “GSM-Med”). The new set of spectral parameters, derived from BOUSSOLE data within the first optical depth, is shown in Table 2. Similar to the approaches proposed by Matsuoka et al. (2013) and Werdell et al. (2013),  $a^*_{\text{phy}}(\lambda)$  coefficients varied as a function of [Tchl  $a$ ] and BOUSSOLE-derived parameterizations based on 567 samples collected from 2003 to 2012 (Table 2). This is more realistic than constant  $a^*_{\text{phy}}(\lambda)$  values because phytoplankton light absorption properties are affected by changes in the algal community size structure and pigment composition (Bricaud et al., 2004; Organelli et al., 2011) as well as their physiological state (Kiefer et al., 1979; Stramski and Morel, 1990). Contrary to  $a^*_{\text{phy}}(\lambda)$ , both the  $\gamma$  and  $S_{\text{cdm}}$  parameters were set to fixed values in GSM-Med (Table 2). These values are the averages of *in situ* values within the first optical depth at the BOUSSOLE site between 2008 and 2011 ( $n = 959$ ) and 2011–2012 ( $n = 30$ ) for the  $\gamma$  and  $S_{\text{cdm}}$  parameters, respectively. This choice was based on evidence that  $\gamma$  and  $S_{\text{cdm}}$  are weakly correlated to variables such as [Tchl  $a$ ] at the BOUSSOLE site (Antoine et al., 2011; Organelli et al., 2014), and are thus difficult to model.

**Table 2**

Set of relationships and parameters measured at the BOUSSOLE site and used for the development of GSM-Med. The set of parameters used by GSM as updated by Maritorena et al. (2002; GSM01) is shown for comparison (right column). From top to bottom: the chlorophyll-specific phytoplankton light absorption coefficients at various wavelengths ( $a^*_{\text{phy}}(\lambda)$ ), the spectral slopes of particle backscattering ( $\gamma$ ) and CDM light absorption values ( $S_{\text{cdm}}$ ). The parameterizations of phytoplankton absorption coefficients for GSM-Med have been derived over the total chlorophyll range ( $0.047\text{--}5.095 \text{ mg m}^{-3}$ ) measured at the BOUSSOLE site between 2003 and 2012.

Parameter	GSM-Med				n	GSM01	
	$A(\lambda) [\text{Tchl } a]^{-B(\lambda)}$					Constant values	
	$\lambda$	A	B	$r^2$		$\lambda$	
$a^*_{\text{phy}}(\lambda)$ ( $\text{m}^2 \text{ mg Tchl } a^{-1}$ )	412	0.04044	0.27629	0.88	567	412	0.00665
	443	0.05165	0.27318	0.89	567	443	0.05582
	490	0.03318	0.29869	0.89	567	490	0.02055
	510	0.02008	0.27730	0.90	567	510	0.01910
	555	0.00690	0.20127	0.85	567	555	0.01015
	670	0.02195	0.18239	0.94	567	670	0.01424
$\gamma$	2.158 $\pm$ 0.53 ( $n = 959$ )					1.0337	
$S_{\text{cdm}}$ ( $\text{nm}^{-1}$ )	0.01664 $\pm$ 0.0014 ( $n = 30$ )					0.0206	

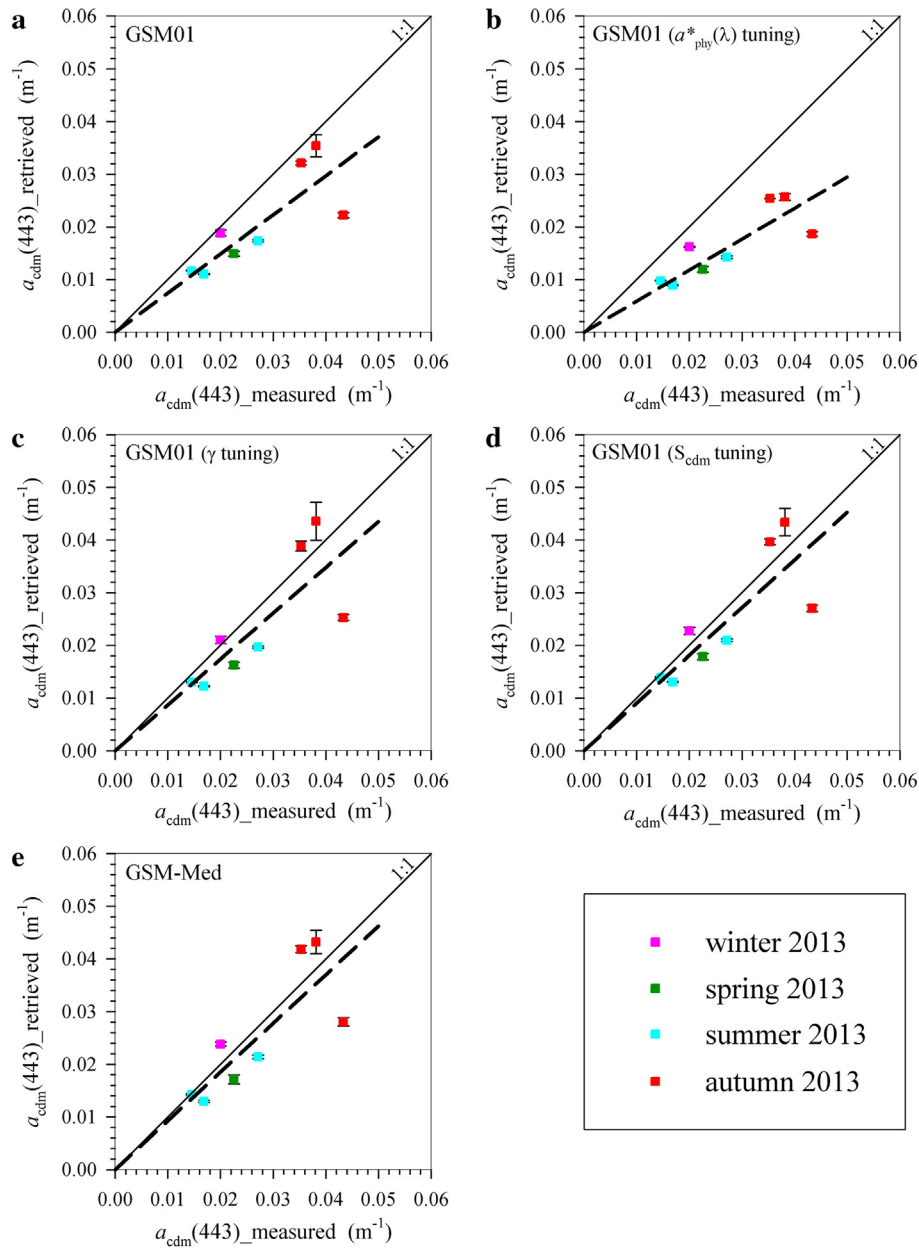


**Fig. 5.** The  $a_{\text{cdm}}(443)$  values derived from radiometric measurements (C-OPS) as a function of those measured from water samples at the BOUSSOLE site (January 2013–December 2013), for the following configurations of the GSM algorithm: a) GSM01 (updated by Maritorea et al., 2002); b) GSM01 using locally-tuned  $a_{\text{phy}}^*(\lambda)$  values; c) GSM01 using a locally-tuned  $\gamma$  parameter; d) GSM01 using a locally-tuned  $S_{\text{cdm}}$  parameter; and e) GSM-Med (i.e., with all tuned parameters). See Table 2 for details of parameters tuned to the BOUSSOLE time-series. Each  $a_{\text{cdm}}(443)$  estimate is the average value for at least three independent  $R_{\text{rs}}(\lambda)$  measurements and error bars are the standard deviation values. In each plot, the solid line is the 1:1 line and the dashed line is a linear fit to all points. Regression statistics are displayed in Table 3.

**Table 3**

Regression statistics for the GSM01 sensitivity analysis using locally-tuned parameters (see Section 2.4 for definitions).

Method	n	b (y = bx)	$r^2$	p-Value	$S_{\text{err}}$	RMSE	MPD	$\text{RMSE}_{\log}$
GSM01	8	0.742	0.95	<0.001	0.068	0.009	26.78%	0.183
GSM01 ( $a_{\text{phy}}^*(\lambda)$ tuning)	8	0.589	0.96	<0.001	0.047	0.012	39.72%	0.275
GSM01 ( $\gamma$ tuning)	8	0.870	0.93	<0.001	0.089	0.008	20.73%	0.142
GSM01 (seasonal $\gamma$ tuning)	8	0.894	0.92	<0.001	0.094	0.008	22.18%	0.138
GSM01 ( $S_{\text{cdm}}$ tuning)	8	0.905	0.94	<0.001	0.084	0.007	17.26%	0.119
GSM01 ( $a_{\text{phy}}^*(\lambda)$ & $\gamma$ tuning)	8	0.720	0.94	<0.001	0.066	0.010	30.35%	0.202
GSM01 ( $a_{\text{phy}}^*(\lambda)$ & $S_{\text{cdm}}$ tuning)	8	0.752	0.95	<0.001	0.062	0.009	24.12%	0.169
GSM01 ( $\gamma$ & $S_{\text{cdm}}$ tuning)	8	1.082	0.93	<0.001	0.113	0.009	19.71%	0.120
GSM-Med	8	0.925	0.94	<0.001	0.087	0.007	20.05%	0.121
GSM-Med (seasonal $S_{\text{cdm}}$ tuning)	8	0.889	0.93	<0.001	0.087	0.007	22.77%	0.134

The sensitivity of GSM01 to locally-tuned coefficients was evaluated by modifying only one of the three parameters ( $a^*_{\text{phy}}(\lambda)$ ,  $\gamma$  or  $S_{\text{cdm}}$ ). The impact on the model results was assessed by varying all of them simultaneously, so that the model assumptions were consistent and representative of the same ecosystem. Because the new spectral coefficients were derived from *in situ* data collected up to 2012, the tuned algorithms were validated using data from 2013 only (Fig. 5; Table 3). The use of tuned  $a^*_{\text{phy}}(\lambda)$  coefficients produced strongly underestimated  $a_{\text{cdm}}(443)$  values (Fig. 5b) and a MPD of 39.72% (Table 3). This is because the new  $a^*_{\text{phy}}(\lambda)$  coefficients returned higher  $a_{\text{phy}}(\lambda)$  values than those obtained from GSM01. Assuming that the total non-water light absorption budget ( $a_{\text{t-w}}(\lambda) = a_{\text{phy}}(\lambda) + a_{\text{cdm}}(\lambda)$ ) did not vary for a given  $R_{\text{rs}}(\lambda)$ ,  $a_{\text{cdm}}(\lambda)$  coefficients were lower when  $a_{\text{phy}}(\lambda)$  increased.

Here, the retrieved  $a_{\text{cdm}}(443)$  values were sensitive to the  $\gamma$  parameter when tuned from the GSM01 to the local value. In contrast, similar results were obtained when using the locally-tuned average  $\gamma$  (Fig. 5c; Table 3) or seasonally-varying  $\gamma$  values (Table 3). These results suggested that main impact on retrievals was due to the increase of the  $\gamma$  value of about 100% with respect to GSM01. Seasonal variations around the local  $\gamma$  parameter induced, instead, only weak changes in  $a_{\text{cdm}}(443)$  retrievals. This was also previously observed by Werdell et al. (2013) where  $\pm 33\%$  variations in the  $\gamma$  parameter (estimated as a function of

$R_{\text{rs}}$ ; Lee et al., 2002) yielded a negligible impact on the accuracy of IOP retrievals.

The tuning of  $S_{\text{cdm}}$  produced the most positive impact on estimating  $a_{\text{cdm}}(443)$  coefficients (Fig. 5d, Table 3), as the regression slope significantly increased (from 0.742 to 0.905), while RMSE and MPD values decreased with respect to the GSM01 (Table 3). The sensitivity of GSM01 to changes in two locally-tuned coefficients at the same time was also evaluated. The tuning of  $a^*_{\text{phy}}(\lambda)$  coefficients together with  $\gamma$  or  $S_{\text{cdm}}$  still yielded underestimated  $a_{\text{cdm}}(443)$  coefficients (Table 3). When tuning  $\gamma$  and  $S_{\text{cdm}}$  parameters simultaneously, the error decreased with respect to GSM01 (Table 3).

The accuracy of the retrieved  $a_{\text{cdm}}(443)$  improved when GSM01 was run with locally-tuned values for  $a^*_{\text{phy}}(\lambda)$ ,  $\gamma$  and  $S_{\text{cdm}}$  simultaneously (GSM-Med, Fig. 5e, Tables 2 & 3). The regression slope was close to the identity line ( $p < 0.05$ ) and MPD was 20.05% (Table 3). This indicates that the spectral components compensated for their respective errors when they were consistent and representative of a given ecosystem. Statistics obtained with this configuration were, however, close to those obtained when only  $S_{\text{cdm}}$  was changed (Table 3). The spectral dependency of CDM absorption was therefore critical for obtaining accurate retrievals of  $a_{\text{cdm}}(443)$  coefficients. Hence, a test was conducted to verify if the accuracy of GSM-Med improved by allowing the  $S_{\text{cdm}}$  parameter to vary seasonally (an average  $S_{\text{cdm}}$  value for each season was

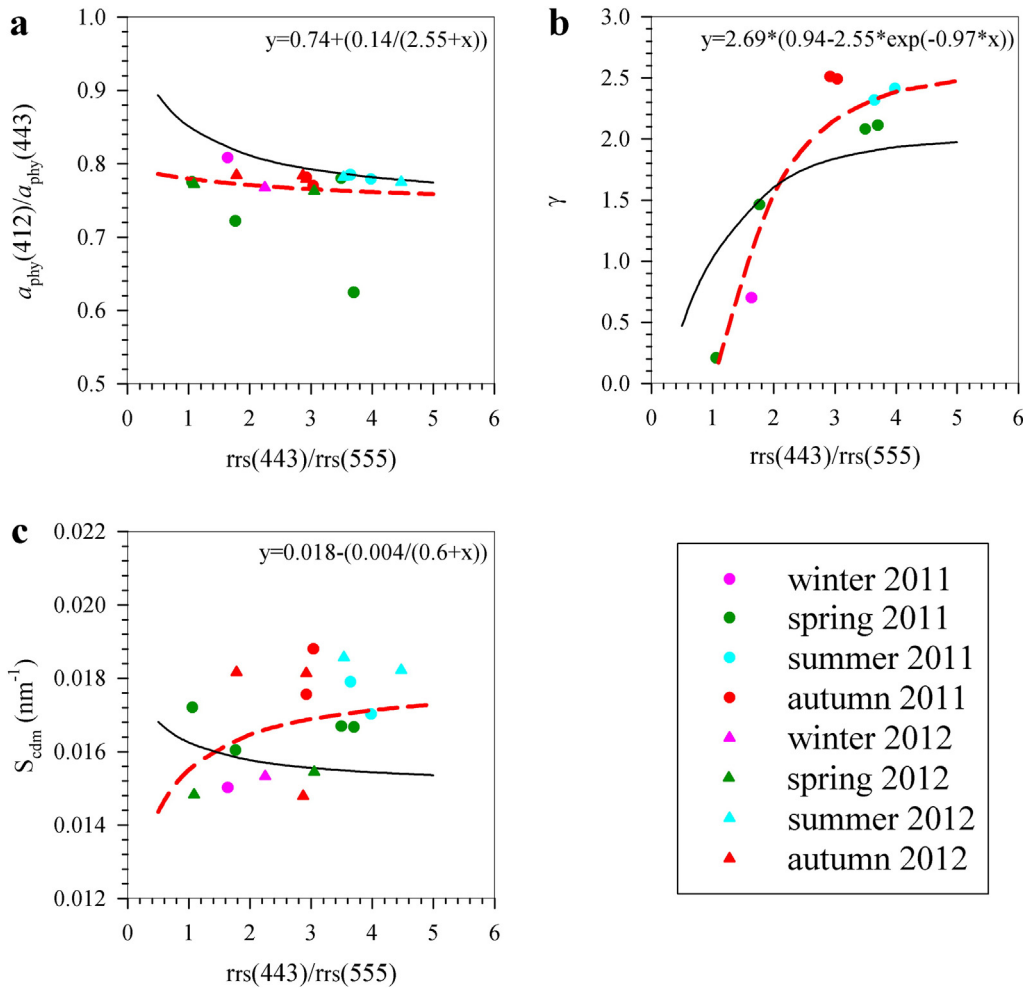


**Fig. 6.** a–c) Empirical relationships at the BOUSSOLE site of  $a_{\text{phy}}(412)/a_{\text{phy}}(443)$ ,  $\gamma$  and  $S_{\text{cdm}}$  spectral parameters, respectively, as a function of the ratio between in-water remote sensing reflectance ( $r_{\text{rs}}$ ) at 443 and 555 nm. In each plot, the solid line is the empirical relationship used in QAAv6 and the dashed line is the optimized fit to all points. Coefficients of the BOUSSOLE-tuned empirical parameterizations are also shown.

used). The MPD value increased by about 3% and the regression slope with *in situ* data decreased (Table 3).

### 3.2. QAAv6

The QAAv6 (Lee et al., 2009) showed the best accuracy for the three years of the BOUSSOLE time-series and the lowest RMSE and MPD values (Fig. 2b; Table 1). Predicted  $a_{\text{cdm}}(443)$  values were significantly correlated with the measured values ( $r^2 = 0.94$ ,  $p < 0.001$ ) and near the identity line ( $p < 0.05$ ) as shown by the regression slope ( $b = 0.981$ ; Table 1). QAAv6 also returned the highest number of valid retrievals (99%). Accurate  $a_{\text{cdm}}(443)$  estimates were obtained during all seasons and even in summer when the CDOM content at the sea surface

was the lowest (Organelli et al., 2014). The error in log-transformed  $a_{\text{cdm}}(443)$  values ( $\text{RMSE}_{\log} = 0.109$ ) for QAAv6 was similar to that found by the IOCCG for a simulated dataset ( $\text{RMSE}_{\log} = 0.093$ ; IOCCG, 2006), while it was half the error found in the *in situ* dataset ( $\text{RMSE}_{\log} = 0.221$ ; IOCCG, 2006).

Using an approach similar to the local tuning of GSM01 model coefficients, the empirical parameterizations used in the QAAv6 inversion ( $a_{\text{phy}}(412)/a_{\text{phy}}(443)$ ,  $\gamma$  and  $S_{\text{cdm}}$  as a function of the ratio of remote sensing reflectance below the water at two wavelengths,  $r_{\text{rs}}(443)/r_{\text{rs}}(555)$ ; Lee et al., 2009) were tuned for the BOUSSOLE site and the model results were evaluated. The appropriateness of these empirical relationships was verified using 2011 and 2012 data for  $a_{\text{phy}}(412)/a_{\text{phy}}(443)$  and  $S_{\text{cdm}}$  and 2011 data only for  $\gamma$  (adapted to the

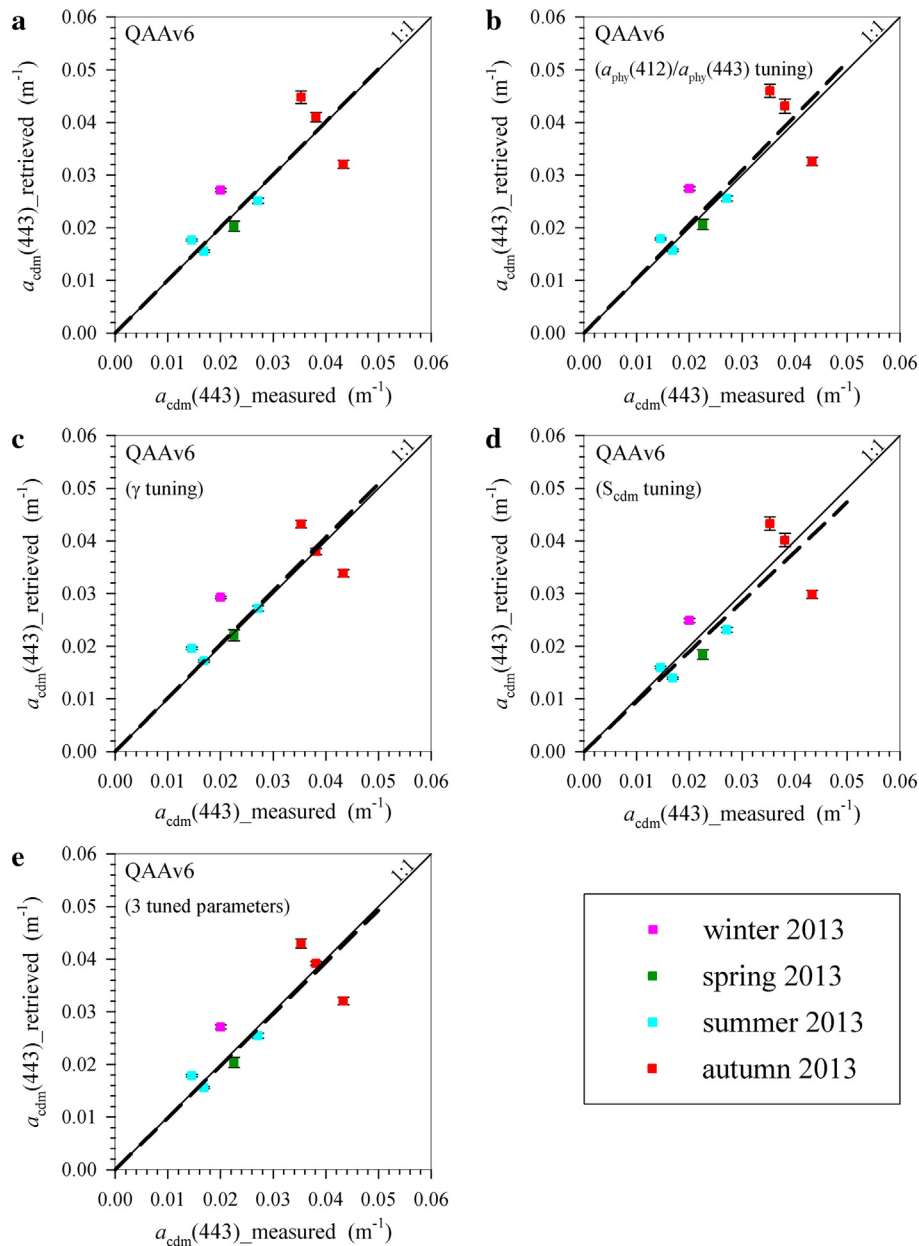


**Fig. 7.** The  $a_{\text{cdm}}(443)$  values derived from radiometric measurements (C-OPS) as a function of those measured from water samples at the BOUSSOLE site (January 2013–December 2013), for the following configurations of the QAAv6 algorithm: a) QAAv6; b) QAAv6 using the locally-tuned empirical relationship for the  $a_{\text{phy}}(412)/a_{\text{phy}}(443)$  parameter; c) QAAv6 using the locally-tuned empirical relationship for the  $\gamma$  parameter; d) QAAv6 using the locally-tuned empirical relationship for the  $S_{\text{cdm}}$  parameter; and e) QAAv6 using the locally-tuned empirical relationships for  $a_{\text{phy}}(412)/a_{\text{phy}}(443)$ ,  $\gamma$  and  $S_{\text{cdm}}$  spectral parameters. Each  $a_{\text{cdm}}(443)$  estimate is the average value for at least three independent  $R_{\text{rs}}(\lambda)$  measurements and error bars are the standard deviation values. In each plot, the solid line is the 1:1 line and the dashed line is a linear fit to all points. Regression statistics are displayed in Table 4.

**Table 4**  
Statistics for match-up analyses shown in Fig. 7 (see Section 2.4 for definitions).

Method	n	b ( $y = bx$ )	$r^2$	p-Value	$S_{err}$	RMSE	MPD	RMSE <sub>log</sub>
QAAv6	8	1.003	0.96	<0.001	0.079	0.006	15.90%	0.098
QAAv6 ( $a_{phy}(412)/a_{phy}(443)$ tuning)	8	1.029	0.96	<0.001	0.083	0.006	18.11%	0.101
QAAv6 ( $\gamma$ tuning)	8	1.017	0.96	<0.001	0.075	0.006	12.06%	0.103
QAAv6 ( $S_{cdm}$ tuning)	8	0.947	0.95	<0.001	0.079	0.006	17.74%	0.103
QAAv6 ( $a_{phy}(412)/a_{phy}(443)$ & $\gamma$ & $S_{cdm}$ tuning)	8	0.985	0.96	<0.001	0.074	0.006	15.76%	0.095

wavelengths 443 and 555 nm as in Lee et al., 2002). These data were collected within the first optical depth. All of the three tuned empirical relationships differed from those used in QAAv6 (Lee et al., 2009; Fig. 6). The  $a_{phy}(412)/a_{phy}(443)$  values changed little for  $r_{rs}(443)/r_{rs}(555)$  ratios varying between 1 and 5 at the BOUSSOLE site, and the tuned parameterization differed from the standard QAAv6 relationship mostly at low  $r_{rs}(443)/r_{rs}(555)$  ratios (Fig. 6a). Good agreement between the tuned and the QAAv6  $\gamma$  versus  $r_{rs}(443)/r_{rs}(555)$  relationships was observed only for  $r_{rs}(443)/r_{rs}(555)$  ratios around 1.7 (Fig. 6b). The  $S_{cdm}$  versus  $r_{rs}(443)/r_{rs}(555)$  parameterization tuned to BOUSSOLE data had an opposite trend as compared to that assumed by QAAv6 (Fig. 6c). The tendency of  $S_{cdm}$  to increase with increasing  $r_{rs}(443)/r_{rs}(555)$  ratios was driven by samples collected at the BOUSSOLE site during the late spring, summer and autumn and influenced by the photobleaching of CDOM (Organelli et al., 2014).

No significant change in the accuracy of QAAv6 was observed when using local parameterizations (Fig. 7; Table 4). From match-up analyses, the regression slopes were near 1 (Table 4) and all RMSE values were  $0.006 \text{ m}^{-1}$  (Table 4). However, when tuning  $S_{cdm}$  alone, the regression slope decreased from 1.003 to 0.947 (Fig. 7d; Table 4). In contrast to  $S_{cdm}$ , the use of tuned relationships for  $a_{phy}(412)/a_{phy}(443)$  and  $\gamma$  yielded regression slopes slightly higher than 1 (Fig. 7b, c; Table 4).

When the three regionally-tuned parameterizations simultaneously replaced those of QAAv6, the three spectral parameters mutually compensated for their opposite effects and the results were similar to those obtained using the standard version (Fig. 7a, e, Table 4). Hence, QAAv6 appears robust against local deviations of bio-optical relationships and can be applied regardless of any local tuning, at least for Case-1 waters such as those encountered at the BOUSSOLE site.

### 3.3. $CB_{QAA}$

The  $CB_{QAA}$  overestimated *in situ*  $a_{cdm}(443)$  values from *in situ*  $R_{rs}(\lambda)$  measurements (Fig. 2c; Table 1). The MPD value and the error for log-transformed quantities were, however, lower than that found for GSM01 (Table 1) and close to that of GSM-Med (Table 3). Because  $CB_{QAA}$  is based on a non-linear optimization technique that simultaneously calculates three output variables ( $a_{cdm}(443)$ ,  $S_{cdm}$  and  $S_f$ ; Ciotti and Bricaud, 2006) and no empirical relationship is used, no local tuning can be performed.  $CB_{QAA}$  also had a lower percentage of valid retrievals than the other algorithms (Table 1). This was caused by the 5% tolerance error imposed for comparisons between measured and modeled  $R_{rs}(\lambda)$  spectra (Ciotti and Bricaud, 2006; Bricaud et al., 2012).

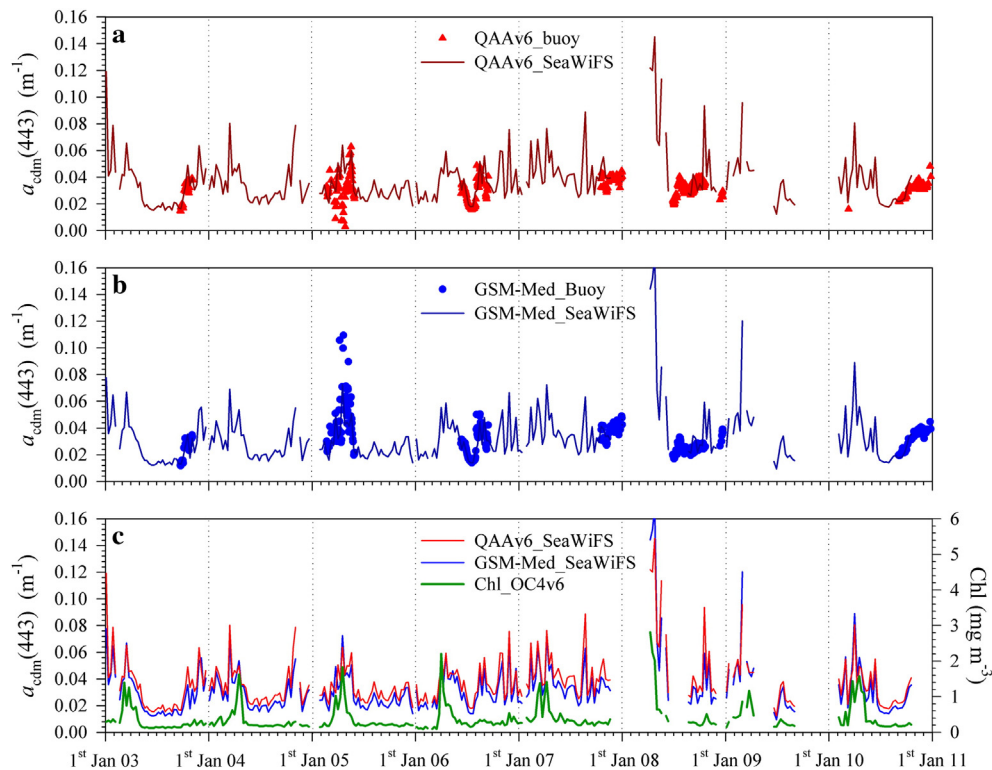


**Fig. 8.** a) Time-series at the BOUSSOLE site (January 2003–December 2010) of SeaWiFS-derived  $a_{cdm}(443)$  estimates using the QAAv6, onto which the buoy-derived values are superimposed. b) Same time-series as in (a) but for SeaWiFS-derived  $a_{cdm}(443)$  values using GSM-Med, onto which the buoy-derived values are superimposed. c) Same time-series as in (a) but for SeaWiFS-derived  $a_{cdm}(443)$  values using the QAAv6 and the GSM-Med algorithms, onto which the SeaWiFS-derived chlorophyll concentrations are superimposed.

The  $CB_{QAA}$ , however, showed improved accuracy in retrieving the  $a_{cdm}(443)$  values with respect to the previous version by Bricaud et al. (2012) owing to the use of more accurate estimates of the total non-water light absorption coefficients ( $a_{t-w}(\lambda)$ ). Indeed, the QAAv6 used in  $CB_{QAA}$  yielded more accurate estimates of  $a_{t-w}(\lambda)$  coefficients over the entire BOUSSOLE time-series ( $b = 1.05$ ,  $r^2 = 0.98$ ,  $n = 30$ ,  $p < 0.001$ ,  $S_{err} = 0.027$ ,  $RMSE = 0.008 \text{ m}^{-1}$ ,  $MPD = 10.48\%$ ) than the Loisel and Stramski (2000) algorithm ( $b = 0.89$ ,  $r^2 = 0.95$ ,  $n = 27$ ,  $p < 0.001$ ,  $S_{err} = 0.039$ ,  $RMSE = 0.012 \text{ m}^{-1}$ ,  $MPD = 14.05\%$ ) used in CB2012 (see Section 2.4 for details). The  $a_{cdm}(443)$  coefficients were strongly underestimated by CB2012 over the entire BOUSSOLE time-series ( $b = 0.766$ ,  $r^2 = 0.78$ ,  $n = 27$ ,  $p < 0.001$ ,  $S_{err} = 0.079$ ; data not shown) with RMSE and MPD values of  $0.014 \text{ m}^{-1}$  and 42.95%, respectively.

### 3.4. Time-series of satellite-derived $a_{cdm}(443)$ coefficients

The eight-year time-series of  $a_{cdm}(443)$  coefficients retrieved from SeaWiFS remote sensing reflectance spectra (September 2003–December 2010) using the two best algorithms for the BOUSSOLE site, QAAv6 and GSM-Med, were consistent with the *in situ* buoy measurements (Fig. 8a, b). Satellite-derived reconstructions of  $a_{cdm}(443)$  coefficients reproduced similar seasonal dynamics (Fig. 8c), which were also close to observed *in situ* CDOM only (Organelli et al., 2014). This suggests that satellite-derived time-series of  $a_{cdm}(443)$  coefficients can be used to investigate patterns of  $a_{cdm}(443)$  and of phytoplankton chlorophyll

concentrations at the BOUSSOLE site. GSM-Med  $a_{cdm}(443)$  estimates were, however, significantly lower than those retrieved with QAAv6 ( $y = 0.90x$ ,  $r^2 = 0.97$ ,  $n = 290$ ,  $p < 0.001$ ,  $S_{err} = 0.009$ ,  $RMSE = 0.008 \text{ m}^{-1}$ ,  $MPD = 18.29\%$ ; Fig. 9a).

In agreement with *in situ* observations (Organelli et al., 2014), the highest  $a_{cdm}(443)$  values were typically observed following the spring algal bloom (Fig. 8c). Satellite-derived  $a_{cdm}(443)$  coefficients generally decreased towards summer (Fig. 8c) because of photobleaching (Organelli et al., 2014), while a second relative maximum was observed in autumn and early winter (Fig. 8c) as a consequence of a fall bloom such as in 2008 (Fig. 8c) or more likely of the upwelling of deep, biologically refractory CDOM (Nelson and Siegel, 2013).

SeaWiFS-derived  $a_{cdm}(443)$  coefficients at the BOUSSOLE site were higher than the  $a_{cdm}(443)$  versus total chlorophyll relationships proposed by Bricaud et al. (2012) for various seasons at the global scale, except during the spring algal bloom (Fig. 9b, c). This is due to the higher-than-average contribution of CDOM for a given chlorophyll concentration in the Mediterranean Sea, which makes the optical properties of this basin different from many oceanic areas (Morel and Gentili, 2009b; Organelli et al., 2014). Co-variation of  $a_{cdm}(443)$  with the satellite-derived chlorophyll concentrations was found for QAAv6 ( $r^2 = 0.48$ ,  $n = 290$ ,  $p < 0.001$ ; Fig. 9b) and GSM-Med ( $r^2 = 0.58$ ,  $n = 290$ ,  $p < 0.001$ ; Fig. 9c), but with high scatter. This was likely an effect of the varying seasonal influence of photobleaching and a consequence of the time lag between chlorophyll and CDOM maxima (Organelli et al., 2014). Cross-correlation analysis between QAAv6- or GSM-Med-

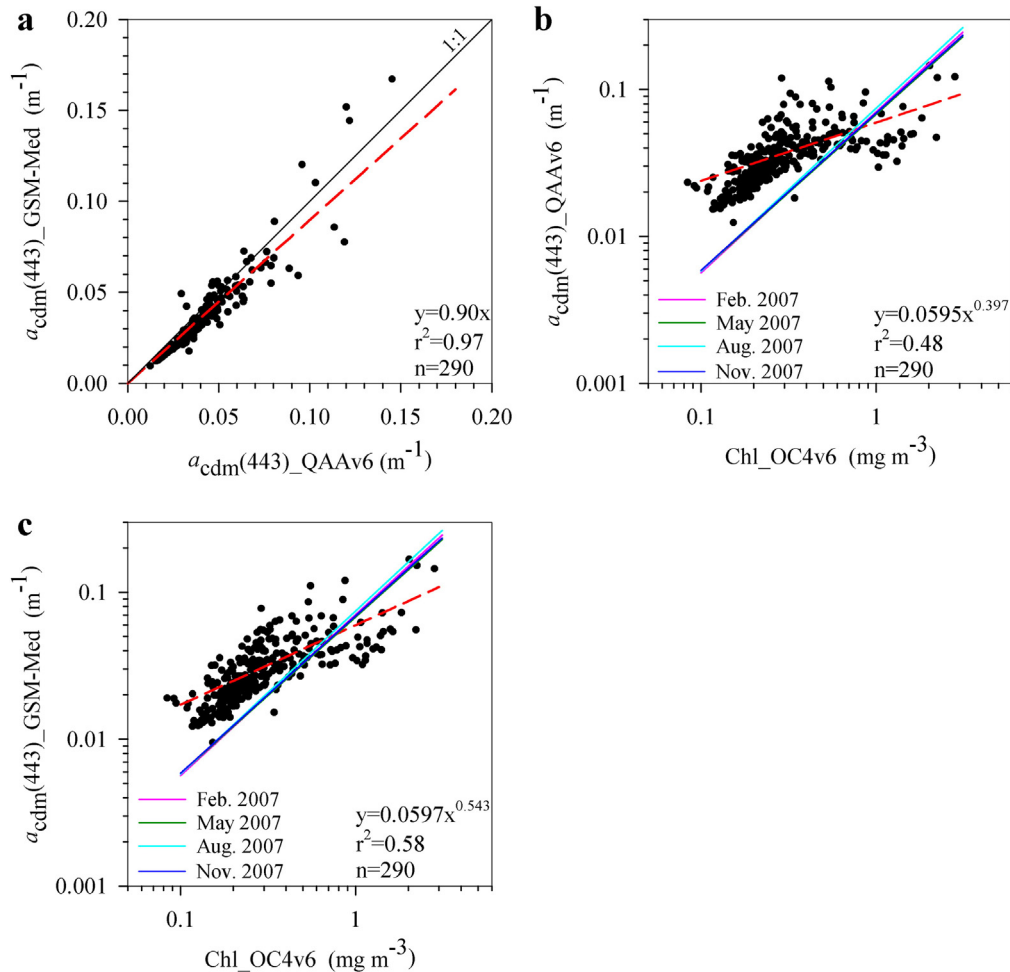


**Fig. 9.** a) Comparison between SeaWiFS  $a_{cdm}(443)$  values as derived from GSM-Med and the QAAv6 algorithms. The linear fit to all points (dashed line) and the 1:1 line (solid line) are displayed. b) Variations of QAAv6-derived  $a_{cdm}(443)$  values as a function of chlorophyll concentrations, both derived from SeaWiFS data. c) as in b) but for  $a_{cdm}(443)$  values as derived from the GSM-Med method. In panels b) and c) non-least square fit to all points (dashed line) and global relationships for four months (February, May, August and November 2007) from Bricaud et al. (2012) are displayed.

derived  $a_{\text{cdm}}(443)$  coefficients and OC4-derived chlorophyll concentrations confirmed that CDM increased generally within one month of the chlorophyll maximum (correlation coefficients up to 0.83,  $p < 0.05$ ), likely due to microbial decomposition of phytoplankton cells (Organelli et al., 2014) or excretion by zooplankton (Steinberg et al., 2004; Kitidis et al., 2006; Xing et al., 2014).

#### 4. Conclusions

This study showed that two semi-analytical models (GSM-Med, QAAv6) accurately retrieved  $a_{\text{cdm}}(443)$  coefficients at the BOUSSOLE site in the NW Mediterranean Sea, while the CB<sub>QAA</sub> algorithm tended to overestimate *in situ*  $a_{\text{cdm}}(443)$  coefficients. QAAv6 was the most robust method for retrieving  $a_{\text{cdm}}(443)$  coefficients at the BOUSSOLE site. Local bio-optical relationships that differed from those in the model did not strongly impact retrieval error. GSM01 was more strongly affected by deviations from globally derived parameters or relationships. The locally-tuned version, GSM-Med, showed improved  $a_{\text{cdm}}(443)$  estimates with an accuracy comparable to QAAv6.

Satellite-derived reconstruction of  $a_{\text{cdm}}(443)$  over an eight-year time-series at the BOUSSOLE site reproduced seasonal patterns similar to those observed in the same area by Organelli et al. (2014) and Xing et al. (2014). More importantly, remotely-retrieved  $a_{\text{cdm}}(443)$  coefficients revealed that the CDM light absorption, for a given chlorophyll concentration, at the BOUSSOLE site was higher than the open ocean global average observed by Bricaud et al. (2012).

The retrieval of accurate  $a_{\text{cdm}}(443)$  values and the assessment of dynamics from space can improve our understanding of the carbon cycle as well as tracing processes (Nelson et al., 2010) and changes (Siegel et al., 2013) in ocean biogeochemistry. To extend this investigation at the basin scale, future efforts should evaluate algorithms and validate the retrievals of  $a_{\text{cdm}}(\lambda)$  coefficients and other bio-optical products (e.g.,  $a_{\text{phy}}(\lambda)$  coefficients) across the entire Mediterranean Sea, as well as to better understand the forcing behind changes in the  $a_{\text{cdm}}(\lambda)$  and  $S_{\text{cdm}}$  parameters. Furthermore, the models we tested were only adapted to the SeaWiFS spectral resolution, and efforts should be made to test and validate algorithms for current (e.g., NASA's MODIS-Aqua and ESA's Sentinel 3) and future (e.g., NASA's PACE) satellite platforms. The development of methods based on hyperspectral or UV-visible multispectral measurements could be useful to more accurately estimate the spectral dependence of CDM, which is a useful proxy (if NAP  $\ll$  CDOM) of the origin of CDOM (Carder et al., 1989; Vodacek et al., 1997) and a tracer of photochemical/microbial degradation processes (Green and Blough, 1994; Moran et al., 2000; Helms et al., 2008).

#### Acknowledgements

We thank the BOUSSOLE technical staff ([http://www.obs-vlfr.fr/Boussole/html/people/tech\\_staff.php](http://www.obs-vlfr.fr/Boussole/html/people/tech_staff.php)) and the captains and crews of the R/V (*Téthys-II*, *Antea* and *Europe*) operating the monthly cruises. In particular, we are grateful to Emilie Diamond and Melek Golbol for *in situ* measurements and to Joséphine Ras and Mustapha Ouhssain for the HPLC pigment and particulate absorption analyses. This study is a contribution to the BIOCAREX project, which was funded by the Agence Nationale de la Recherche (ANR, Paris), and to the BOUSSOLE project, which was funded by the European Space Agency (ESA; Grant No.: 4000102992/11/I-NB) and Centre National d'Etudes Spatiales (CNES). We thank the organizations that provided technical and logistical support to the BOUSSOLE project: Centre National de la Recherche Scientifique (CNRS), Institut National des Sciences de l'Univers (INSU), Université Pierre et Marie Curie (UPMC), and the Observatoire Océanologique de Villefranche sur Mer (OOV). We are grateful to Catherine Brown for improving the English of the manuscript. We also thank the two anonymous reviewers for their comments and suggestions.

#### References

- Antoine, D., Chami, M., Claustre, H., D'Ortenzio, F., Morel, A., Bécu, G., Gentili, B., Louis, F., Ras, J., Roussier, E., Scott, A.J., Tailliez, D., Hooker, S.B., Guevel, P., Desté, J.F., Dempsey, C., Adams, D., 2006. BOUSSOLE: A Joint CNRS-INSU, ESA, CNES and NASA Ocean Color Calibration and Validation Activity, NASA Technical Memorandum No. 2006-214147. NASA Goddard Space Flight Center, Greenbelt.
- Antoine, D., D'Ortenzio, F., Hooker, S.B., Bécu, G., Gentili, B., Tailliez, D., Scott, A.J., 2008. Assessment of uncertainty in the ocean reflectance determined by three satellite ocean color sensors (MERIS, SeaWiFS and MODIS-A) at an offshore site in the Mediterranean Sea (BOUSSOLE project). *J. Geophys. Res.* 113, C07013. <http://dx.doi.org/10.1029/2007JC004472>.
- Antoine, D., Siegel, D.A., Kostadinov, T., Maritorena, S., Nelson, N.B., Gentili, B., Vellucci, V., Guillocheau, N., 2011. Variability in optical particle backscattering in contrasting bio-optical oceanic regimes. *Limnol. Oceanogr.* 56 (3), 955–973.
- Babin, M., Stramski, D., Ferrari, G.M., Claustre, H., Bricaud, A., Obolensky, G., Hoepffner, N., 2003. Variations in the light absorption coefficients of phytoplankton, nonalgal particles, and dissolved organic matter in coastal waters around Europe. *J. Geophys. Res.* 108 (C7), 3211. <http://dx.doi.org/10.1029/2001JC000882>.
- Bélangier, S., Babin, M., Larouche, P., 2008. An empirical ocean color algorithm for estimating the contribution of chromophoric dissolved organic matter to total light absorption in optically complex waters. *J. Geophys. Res.* 113, C04027. <http://dx.doi.org/10.1029/2007JC004436>.
- Boss, E., Roesler, C., 2006. Over constrained linear matrix inversion with statistical selection. In: Lee, Z.P. (Ed.), *Remote Sensing of Inherent Optical Properties: Fundamentals, Test of Algorithms, and Applications*, Reports of the International Ocean-Colour Coordinating Groups No. 5. IOCCG, Dartmouth, pp. 57–62.
- Bricaud, A., Stramski, D., 1990. Spectral absorption coefficients of living phytoplankton and nonalgal biogenous matter: a comparison between Peru upwelling area and Sargasso Sea. *Limnol. Oceanogr.* 35, 562–582.
- Bricaud, A., Morel, A., Prieur, L., 1981. Absorption by dissolved organic matter of the sea (yellow substance) in the UV and visible domains. *Limnol. Oceanogr.* 26 (1), 43–53.
- Bricaud, A., Babin, M., Morel, A., Claustre, H., 1995. Variability in the chlorophyll-specific absorption coefficients of natural phytoplankton: analysis and parameterization. *J. Geophys. Res.* 100, 13321–13332.
- Bricaud, A., Morel, A., Babin, M., Allali, K., Claustre, H., 1998. Variations of light absorption by suspended particles with chlorophyll *a* concentration in oceanic (case 1) waters: analysis and implications for bio-optical models. *J. Geophys. Res.* 103, 31033–31044.
- Bricaud, A., Claustre, H., Ras, J., Oubelkheir, K., 2004. Natural variability of phytoplanktonic absorption in oceanic waters: influence of the size structure of algal populations. *J. Geophys. Res.* 109, C11010.
- Bricaud, A., Ciotti, A.M., Gentili, B., 2012. Spatial-temporal variations in phytoplankton size and colored detrital matter absorption at global and regional scales, as derived from twelve years of SeaWiFS data (1998–2009). *Glob. Biogeochem. Cycles* 26, GB1010. <http://dx.doi.org/10.1029/2010GB003952>.
- Brown, C.A., Huot, Y., Werdell, J.P., Gentili, B., Claustre, H., 2008. The origin and global distribution of second order variability in satellite ocean color and its potential applications to algorithm development. *Remote Sens. Environ.* 112, 4186–4203. <http://dx.doi.org/10.1016/j.rse.2008.06.008>.
- Cao, F., Miller, W.L., 2015. A new algorithm to retrieve chromophoric dissolved organic matter (CDOM) absorption spectra in the UV from ocean color. *J. Geophys. Res.* Oceans 120, 496–516. <http://dx.doi.org/10.1002/2014JC010241>.
- Carder, K.L., Steward, R.G., Harvey, G.R., Ortner, P.B., 1989. Marine humic and fulvic acids: their effects on remote sensing of ocean chlorophyll. *Limnol. Oceanogr.* 34, 68–81.
- Carder, K.L., Chen, F.R., Lee, Z.P., Hawes, S.K., Kamykowski, D., 1999. Semianalytic moderate-resolution imaging spectrometer algorithms for chlorophyll-*a* and absorption with bio-optical domains based on nitrate-depletion temperatures. *J. Geophys. Res.* 104, 5403–5421.
- Ciotti, A.M., Bricaud, A., 2006. Retrievals of a size parameter for phytoplankton and spectral light absorption by colored detrital matter from water leaving radiances at SeaWiFS channels in a continental shelf region off Brazil. *Limnol. Oceanogr. Methods* 4, 237–253.
- Ciotti, A.M., Lewis, M.R., Cullen, J.J., 2002. Assessment of the relationships between dominant cell size in natural phytoplankton communities and the spectral shape of the absorption coefficient. *Limnol. Oceanogr.* 47, 404–417.
- Claustre, H., Morel, A., Hooker, S.B., Babin, M., Antoine, D., Oubelkheir, K., Bricaud, A., Leblanc, K., Quéguiner, B., Maritorena, S., 2002. Is desert dust making oligotrophic waters greener? *Geophys. Res. Lett.* 29 (10), 1469. <http://dx.doi.org/10.1029/2001GL014056>.
- Coble, P.G., 2007. Marine optical biogeochemistry: the chemistry of ocean color. *Chem. Rev.* 107, 402–418.
- Devred, E., Sathyendranath, S., Platt, T., 2006. Inversion based on a semi-analytical reflectance model. In: Lee, Z.P. (Ed.), *Remote Sensing of Inherent Optical Properties: Fundamentals, Test of Algorithms, and Applications*, Reports of the International Ocean-Colour Coordinating Groups No. 5. IOCCG, Dartmouth, pp. 87–94.
- Dong, Q., Shang, S., Lee, Z.P., 2013. An algorithm to retrieve absorption coefficient of chromophoric dissolved organic matter from ocean color. *Remote Sens. Environ.* 128, 259–267.
- D'Ortenzio, F., Marullo, S., Ragni, M., Ribera d'Alcalá, M., Santoleri, R., 2002. Validation of empirical SeaWiFS algorithms for chlorophyll-*a* retrieval in the Mediterranean Sea. A case study for oligotrophic seas. *Remote Sens. Environ.* 82, 79–94.
- D'Sa, E., Miller, R.L., 2003. Bio-optical properties in waters influenced by the Mississippi River during low flow conditions. *Remote Sens. Environ.* 84 (4), 538–549. [http://dx.doi.org/10.1016/S0034-4257\(02\)00163-3](http://dx.doi.org/10.1016/S0034-4257(02)00163-3).
- Garver, S.A., Siegel, D., 1997. Inherent optical property inversion of ocean color spectra and its biogeochemical interpretation. 1. Time series from the Sargasso Sea. *J. Geophys. Res.* 102, 18607–18625.

- Gitelson, A., Karnieli, A., Goldman, N., Yacobi, Y.Z., Mayo, M., 1996. Chlorophyll estimation in the southeastern Mediterranean using CZCS images: adaptation of an algorithm and its validation. *J. Mar. Syst.* 9, 283–290.
- Gordon, H., Ding, R., 1992. Self-shading of in-water optical instruments. *Limnol. Oceanogr.* 37, 491–500.
- Gordon, H.R., Brown, O.B., Evans, R.H., Brown, J.W., Smith, R.C., Baker, K.S., Clark, D.K., 1988. A semi-analytical radiance model of ocean color. *J. Geophys. Res.* 93, 10909–10924.
- Green, S.A., Blough, N.V., 1994. Optical absorption and fluorescence properties of chromophoric dissolved organic matter in natural waters. *Limnol. Oceanogr.* 39 (8), 1903–1916.
- Gregg, W.W., Carder, K.L., 1990. A simple spectral solar irradiance model for cloudless maritime atmospheres. *Limnol. Oceanogr.* 35, 1657–1675.
- Helms, J.R., Stubbins, A., Ritchie, J.D., Minor, E.C., Kieber, D.J., Mopper, K., 2008. Absorption spectral slopes and slope ratios as indicators of molecular weight, source, and photobleaching of chromophoric dissolved organic matter. *Limnol. Oceanogr.* 53 (3), 955–969.
- Hoge, F.E., Lyon, P.E., 1996. Satellite retrieval of inherent optical properties by linear matrix inversion of oceanic radiance models: an analysis of model and radiance measurements errors. *J. Geophys. Res.* 101, 16631–16648.
- Hooker, S.B., Esaias, W.E., Feldman, G.C., Gregg, W.W., Mc Clain, C.R., 1992. An overview of SeaWiFS and ocean colour. In: Hooker, S.B., Firestone, E.R. (Eds.), *SeaWiFS Technical Report Series*, NASA Technical Memorandum 104566. NASA Goddard Space Flight Center, Greenbelt.
- Huang, J., Chen, L., Chen, X., Song, Q., 2013. Validation of semi-analytical inversion models for inherent optical properties from ocean color in coastal Yellow Sea and East China Sea. *J. Oceanogr.* 69, 713–725.
- IOCCG, 2006. Remote Sensing of Inherent Optical Properties: Fundamentals, Tests of Algorithms and Applications, Reports of the International Ocean-Colour Coordinating Groups No. 5. IOCCG, Dartmouth.
- Kahru, M., Lee, Z.P., Kudela, R.M., Manzano-Sarabia, M., Mitchell, B.G., 2013. Multi-satellite time series of inherent optical properties in the California current. *Deep-Sea Res. II* <http://dx.doi.org/10.1016/j.dsr2.2013.07.023i>.
- Kiefer, D.A., Olson, R.J., Wilson, W.H., 1979. Reflectance spectroscopy of marine phytoplankton. Part 1. Optical properties as related to age and growth rate. *Limnol. Oceanogr.* 24, 664–672.
- Kitidis, V., Stubbins, A.P., Uher, G., Upstill-Goddard, R.C., Law, C.S., Malcom, E., Woodward, S., 2006. Variability of chromophoric organic matter in surface waters of the Atlantic Ocean. *Deep-Sea Res. II* 53, 1666–1684.
- Kostadinov, T.S., Siegel, D.A., Maritorena, S., Guillocheau, N., 2007. Ocean color observations and modeling for an optically complex site: Santa Barbara Channel, California, USA. *J. Geophys. Res.* 112, C07011. <http://dx.doi.org/10.1029/2006JC003526>.
- Lee, Z.P., Carder, K.L., Arnone, R., 2002. Deriving inherent optical properties from water color: a multi-band quasi-analytical algorithm for optically deep waters. *Appl. Opt.* 41, 5755–5772.
- Lee, Z.P., Weidemann, A., Kindle, J., Arnone, R., Carder, K.L., Davis, C., 2007. Euphotic zone depth: its derivation and implication to ocean-color remote sensing. *J. Geophys. Res.* 112, C03009. <http://dx.doi.org/10.1029/2006JC003802>.
- Lee, Z.P., Lubac, B., Werdell, J., Arnone, R., 2009. An update of the Quasi-Analytical Algorithm (QAA\_v5). [http://www.ioccg.org/groups/Software\\_OCA/QAA\\_v5.pdf](http://www.ioccg.org/groups/Software_OCA/QAA_v5.pdf).
- Loisel, H., Poteau, A., 2006. Inversion of IOP based on Rrs and remotely retrieved Kd. In: Lee, Z.P. (Ed.), *Remote Sensing of Inherent Optical Properties: Fundamentals, Test of Algorithms, and Applications*, Reports of the International Ocean-Colour Coordinating Groups No. 5. IOCCG, Dartmouth, pp. 35–41.
- Loisel, H., Stramski, D., 2000. Estimation of the inherent optical properties of natural waters from irradiance attenuation coefficient and reflectance in the presence of Raman scattering. *Appl. Opt.* 39, 3001–3011. <http://dx.doi.org/10.1364/AO.39.003001>.
- Mannino, A., Russ, M.E., Hooker, S.B., 2008. Algorithm development and validation for satellite-derived distributions of DOC and CDOM in the U.S. Middle Atlantic Bight. *J. Geophys. Res.* 113, C07051. <http://dx.doi.org/10.1029/2007JC004493>.
- Mannino, A., Novak, M.G., Hooker, S.B., Hyde, K., Aurin, D., 2014. Algorithm development and validation of CDOM properties for estuarine and continental shelf waters along the northeastern U.S. coast. *Remote Sens. Environ.* 152, 576–602.
- Maritorena, S., Siegel, D.A., Peterson, A.R., 2002. Optimization of a semi-analytical ocean color model for global-scale applications. *Appl. Opt.* 41 (15), 2705–2714.
- Maritorena, S., Fanton d'Andon, O.H., Mangin, A., Siegel, D.A., 2010. Merged satellite ocean color data products using a bio-optical model: characteristics, benefits and issues. *Remote Sens. Environ.* 114, 1791–1804.
- Maselli, F., Massi, L., Pieri, M., Santini, C., 2009. Spectral angle minimization for the retrieval of optically active seawater constituents from MODIS data. *Photogramm. Eng. Remote Sens.* 75 (5), 595–605.
- Matsuoka, A., Hooker, S.B., Bricaud, A., Gentili, B., Babin, M., 2013. Estimating absorption coefficients of colored chromophoric dissolved organic matter (CDOM) using a semi-analytical algorithm for southern Beaufort Sea waters: application to deriving concentrations of dissolved organic carbon from space. *Biogeosciences* 10, 917–927.
- Mitchell, B.G., 1990. Algorithms for determining the absorption coefficient of aquatic particulates using the quantitative filter technique (QFT). *Ocean Opt.* 137–148.
- Mitchell, B.G., Bricaud, A., Carder, K., Cleveland, J., Ferrari, G., Gould, R., Kahru, M., Kishino, M., Maske, H., Moisan, T., Moore, L., Nelson, N., Phinney, D., Reynolds, R., Sosik, H., Stramski, D., Tassan, S., Trees, C., Weidemann, A., Wieland, J., Vodacek, A., 2000. Determination of spectral absorption coefficients of particles, dissolved material and phytoplankton for discrete water samples. In: Fargion, G.S., Mueller, J.L. (Eds.), *Ocean Optics Protocols for Satellite Ocean Color Sensor Validation*, Rev. 2 NASA Technical Memorandum No. 2000 – 209966. NASA Goddard Space Flight Center, Greenbelt, pp. 125–153.
- Mitchell, B.G., Kahru, M., Wieland, J., Stramska, M., 2002. Determination of spectral absorption coefficients of particles, dissolved material and phytoplankton for discrete water samples. In: Fargion, G.S., Mueller, J.L. (Eds.), *Ocean Optics Protocols for Satellite Ocean Color Sensor Validation*, NASA/TM-2002-210004/Rev3-Vol2. NASA Goddard Space Flight Center, Greenbelt, pp. 231–257.
- Moran, M.A., Sheldon, W.M., Zepp, R.G., 2000. Carbon loss and optical property changes during long-term photochemical and biological degradation of estuarine dissolved organic matter. *Limnol. Oceanogr.* 45 (6), 1254–1264.
- Morel, A., 1988. Optical modeling of the upper ocean in relation to its biogenous matter content (case I waters). *J. Geophys. Res.* 93, 10749–10768.
- Morel, A., Gentili, B., 2009a. A simple band ratio technique to quantify the colored dissolved and detrital organic material from ocean color remotely sensed data. *Remote Sens. Environ.* 113, 998–1011.
- Morel, A., Gentili, B., 2009b. The dissolved yellow substance and the shades of blue in the Mediterranean Sea. *Biogeosciences* 6, 2625–2636.
- Morel, A., Maritorena, S., 2001. Bio-optical properties of oceanic waters: a reappraisal. *J. Geophys. Res.* 106, 7163–7180.
- Morel, A., Prieur, L., 1977. Analysis of variations in ocean color. *Limnol. Oceanogr.* 22, 709–722.
- Morel, A., Antoine, D., Gentili, B., 2002. Bidirectional reflectance of oceanic waters: accounting for Raman emission and varying particle scattering phase function. *Appl. Opt.* 41 (30), 6289–6306.
- Mueller, J.L., Morel, A., Frouin, R., Davis, C., Arnone, R., Carder, K., Lee, Z.P., Steward, R.G., Hooker, S., Mobley, C., McLean, S., Holben, B., Miller, M., Pietras, C., Knobelspiesse, K.D., Fargion, G.S., Porter, J., Voss, K., 2003. Radiometric measurements and data analysis protocols. In: Mueller, J.L., Fargion, G.S., McClain, C.R. (Eds.), *Ocean Optics Protocols for Satellite Ocean Color Sensor Validation*, Rev. 4 Volume 3 NASA Technical Memorandum No. 2003 – 21621. NASA Goddard Space Flight Center, Greenbelt.
- Nagamani, P.V., Chauhan, P., Sanwlani, N., 2011. Comparison of inherent optical properties (IOPs) in open and coastal waters of Arabian Sea using in-situ bio-optical data. *J. Indian Soc. Remote Sens.* 93 (4), 455–462. <http://dx.doi.org/10.1007/s12524-011-0100-8>.
- Nelson, N.B., Siegel, D.A., 2013. The global distribution and dynamics of chromophoric dissolved organic matter. *Ann. Rev. Mar. Sci.* 5, 447–476.
- Nelson, N.B., Siegel, D.A., Carlson, C.A., Swan, C.M., 2010. Tracing global biogeochemical cycles and meridional overturning circulation using chromophoric dissolved organic matter. *Geophys. Res. Lett.* 37, L03610. <http://dx.doi.org/10.1029/2009GL042325>.
- Organelli, E., Nuccio, C., Melillo, C., Massi, L., 2011. Relationships between phytoplankton light absorption, pigment composition and size structure in offshore areas of the Mediterranean Sea. *Adv. Oceanogr. Limnol.* 2, 107–123.
- Organelli, E., Bricaud, A., Antoine, D., Uitz, J., 2013. Multivariate approach for the retrieval of phytoplankton size structure from measured light absorption spectra in the Mediterranean Sea (BOUSSOLE site). *Appl. Opt.* 52 (11), 2257–2273.
- Organelli, E., Bricaud, A., Antoine, D., Matsuoka, A., 2014. Seasonal dynamics of light absorption by chromophoric dissolved organic matter (CDOM) in the NW Mediterranean Sea (BOUSSOLE site). *Deep-Sea Res.* 91, 72–85. <http://dx.doi.org/10.1016/j.dsr.2014.05.003>.
- Ras, J., Uitz, J., Claustre, H., 2008. Spatial variability of phytoplankton pigment distributions in the subtropical South Pacific Ocean: comparison between in situ and modelled data. *Biogeosciences* 5, 353–369.
- Shanmugam, P., 2011. New models for retrieving and partitioning the colored dissolved organic matter in the global ocean: implications for remote sensing. *Remote Sens. Environ.* 115, 1501–1521.
- Shanmugam, P., Ahn, Y.H., Ryu, J.H., Sundarabalan, B., 2010. An evaluation of inversion models for retrieval of inherent optical properties from ocean color in coastal and open sea waters around Korea. *J. Oceanogr.* 66, 815–830.
- Siegel, D.A., Maritorena, S., Nelson, N.B., Hansell, D.A., Lorenzi-Kayser, M., 2002. Global distribution and dynamics of colored dissolved and detrital organic materials. *J. Geophys. Res.* 107 (C12), 3228. <http://dx.doi.org/10.1029/2011JC000965>.
- Siegel, D.A., Maritorena, S., Nelson, N.B., Behrenfeld, M.J., McClain, C.R., 2005. Colored dissolved organic matter and its influence on the satellite-based characterization of the ocean biosphere. *Geophys. Res. Lett.* 32, L20605. <http://dx.doi.org/10.1029/2005GL024310>.
- Siegel, D.A., Behrenfeld, M.J., Maritorena, S., McClain, C.R., Antoine, D., Bailey, S.W., Bontempi, P.S., Boss, E.S., Dierssen, H.M., Doney, S.C., Eplee Jr., R.E., Evans, R.H., Feldman, G.C., Fields, E., Franz, B.A., Kuring, N.A., Mengelt, C., Nelson, N.B., Patt, F.S., Robinson, W.D., Sarmiento, J.L., Swan, C.M., Werdell, P.J., Westberry, T.K., Wilding, J.G., Yoder, J.A., 2013. Regional to global assessments of phytoplankton dynamics from the SeaWiFS mission. *Remote Sens. Environ.* 135, 77–91.
- Steinberg, D.K., Nelson, N., Carlson, C.A., Prusak, A.C., 2004. Production of chromophoric dissolved organic matter (CDOM) in the open ocean by zooplankton and the colonial *Cyanobacterium trichodesmium* spp. *Mar. Ecol. Prog. Ser.* 267, 45–56.
- Stramski, D., Morel, A., 1990. Optical properties of photosynthetic picoplankton in different physiological states as affected by growth irradiance. *Deep-Sea Res.* 37 (2), 245–266.
- Vodacek, A., Blough, N.V., DeGrandpre, M.D., Peltzer, E.T., Nelson, R.K., 1997. Seasonal variation of CDOM and DOC in the Middle Atlantic Bight: terrestrial inputs and photooxidation. *Limnol. Oceanogr.* 42 (4), 674–686.
- Werdell, P.J., Franz, B.A., Bailey, S.W., Feldman, G.C., Boss, E., Brando, V.E., Dowell, M., Hirata, T., Lavender, S.J., Lee, Z.P., Loisel, H., Maritorena, S., Mélin, F., Moore, T.S., Smyth, T.J., Antoine, D., Devred, E., Fanton d'Andon, O.H., Mangin, A., 2013. Generalized ocean color inversion model for retrieving marine inherent optical properties. *Appl. Opt.* 52 (10), 2019–2037.
- Xing, X., Claustre, H., Wang, H., Poteau, A., D'Ortenzio, F., 2014. Seasonal dynamics in colored dissolved organic matter in the Mediterranean Sea: patterns and drivers. *Deep-Sea Res.* 83, 93–101.
- Zheng, G., Stramski, D., Reynolds, R.A., 2014. Evaluation of the Quasi-Analytical Algorithm for estimating the inherent optical properties of seawater from ocean color: comparison of Arctic and lower-latitude waters. *Remote Sens. Environ.* 155, 194–209.
- Zhu, W., Yu, Q., Tian, Y.Q., Chen, R.F., Gardner, G.B., 2011. Estimation of chromophoric dissolved organic matter in the Mississippi and Atchafalaya river plume regions using above-surface hyperspectral remote sensing. *J. Geophys. Res.* 116, C02011. <http://dx.doi.org/10.1029/2010JC006523>.